March 2016

Evolvability of the Skull: A Study of Genetic Basis and Integration in the Teleost Craniofacial Skeleton

Yinan Hu
University of Massachusetts - Amherst

EVOLVABILITY OF THE SKULL: A STUDY OF GENETIC BASIS AND INTEGRATION IN THE TELEOST CRANIOFACIAL SKELETON

A Dissertation Presented

by

YINAN HU

Submitted to the Graduate School of the

University of Massachusetts Amherst in partial fulfillment

of the requirements for the degree of

DOCTOR OF PHILOSOPHY

February 2016

Organismic and Evolutionary Biology Program

EVOLVABILITY OF THE SKULL: A STUDY OF GENETIC BASIS AND INTEGRATION IN THE TELEOST CRANIOFACIAL SKELETON

A Dissertation Presented

by

YINAN HU

Approved as to style and content by:

_____
R. Craig Albertson, Chair

_____
Elizabeth R. Dumont, Member

_____
Stephen D. McCormick, Member

_____
William J. Cooper, Member

_____
Elizabeth R. Dumont, Director, Interdisciplinary Graduate Programs
Organismic and Evolutionary Biology

DEDICATION

To my beloved parents.

ACKNOWLEDGEMENTS

I want to thank my advisor, R. Craig Albertson, for all his help over the past six years, for always being patient and supportive. I would like to thank my committee members, Betsy Dumont, Rolf Karlstrom and Steve McCormick, for supporting and guiding my research. I would also like to thank Bill Detrich, for his generous offer of a field trip to Palmer station, Antarctica.

I thank all of the past and current members of the Albertson lab, as well as my fellow graduate students for making my graduate experience fun and enjoyable. And I want to thank Penny Jaques for keeping me on track with all the administrative tasks.

Above all, I would like to thank my wife, Qianzhi Jiang, for taking care of me, for always standing by my side, and for bringing all the fun to our life.

ABSTRACT

EVOLVABILITY OF THE SKULL: A STUDY OF GENETIC BASIS AND INTEGRATION IN THE TELEOST CRANIOFACIAL SKELETON

FEBRUARY 2016

YINAN HU, B.S., NANJING NORMAL UNIVERSITY

Ph.D., UNIVERSITY OF MASSACHUSETTS AMHERST

Directed by: R. Craig Albertson

As the field of evolutionary biology pivots away from a gene-centric view of how adaptive evolution proceeds, renewed emphasis is placed on the origin of phenotypic variation. Understanding the developmental processes that underlie the production of novel traits, and how they might influence evolvability, is considered a primary goal in the on-going "extended evolutionary synthesis". The following dissertation explores these questions in the context of adaptive radiations in fish, with a focus on morphological variation in the craniofacial skeleton. Specifically, the first chapter investigates the genetic and developmental basis of shape (co-)variation in the feeding apparatus of African cichlid fishes, and uncovers a common signaling pathway that underlies the adaptive evolution of multiple elements in a complex functional structure. The second chapter presents a new method that is capable of evaluating phenotypic integration on the individual level, and demonstrates its utility in genetic mapping studies. The third chapter characterizes the pattern of morphological diversification in the Antarctic notothenioid fishes, and discusses how integration might have facilitated their adaptive radiation in the Southern Ocean.

TABLE OF CONTENTS

Page

LIST OF TABLES

Table Page

LIST OF FIGURES

Figure Page

LIST OF ABBREVIATIONS

°C	degree Celsius
3D	three dimensional
AE-Mod	the articular extension module
AFGP	anti-freeze glycoprotein
AIC	Akaike information criterion
A-Mod	the articular module
bp	base pair
bsr	branchiostegal rays
cfr	caudal fin rays
ch	ceratohyal
col10a1	collagen type X alpha 1
col1a1	collagen type I alpha 1
cyc/CyA	cyclopamine
dnt	dentary
dpf	days post-fertilization
e	eye
eth	ethmoid plate
EtOH	ethanol
Evo-Devo	evolutionary developmental biology
FST	fixation index, a measure of genetic differentiation between populations
gli1	GLI family zinc finger 1
Hh	Hedgehog (signaling pathway)
hs	hyosymplectic
IOP	interopercle
iopl/IOPL	interopercular-mandibular ligament
kb	kilo-base pair

KT	kinematic transmission ratio
LF	*Labeotropheus fuelleborni*
LG	linkage group
L-Mod	the lateral line module
LOD	logarithm of the odds
m	Meckel's cartilage
M	molar
MA_O	mechanical advantage of opening
MDI	morphological disparity index
mg	milligram
min	minute
mL	milliliter
mM	millimolar
MQM	Multiple-QTL Mapping
mx	maxilla
MZ	*Maylandia zebra*
no.	number
OU	Ornstein-Uhlenbeck
pap	posterior articulation process
PC	principal component
PCA	principal components analysis
PLS	partial least squares
pmx	premaxilla
pop	preopercle
pq	palatoquadrate
ptch1	patched-1
PVE	percent variance explained
q-PCR	quantitative polymerase chain reaction
QTL	quantitative trait loci

RA	retroarticular process
RAD	restriction site associated DNA markers
RNA	ribonucleic acid
S.E.	standard error
SNP	single nucleotide polymorphism
T.gra	*Tropheops gracilior*
T.int	*Tropheops intermedius*
T.kwazi	*Tropheops* sp. from chinyankwazi
T.wezi	*Tropheops* sp. from chinyamwezi
T-Mod	the tooth-bearing module
TT	*Tropheops tropheops*
Tukey's HSD	Tukey's honest significant difference
VSE	variance of scaled eigenvalues
WISH	Whole-mount *in situ* hybridization
μm	micrometer
μM	micromolar

CHAPTER I

MULTI-LEVEL INTEGRATION UNDERLIES ADAPTIVE VARIATION IN THE CICHLID FEEDING APPARATUS

1.1 Introduction

The current paradigm of evolutionary biology is dominated by a "gene-centric view" of evolution, which is rooted from the successful fusion of Darwin's theory of natural selection and the theory of genetics during the Modern Synthesis. In this view, adaptive evolution occurs via two processes: 1) genetic mutation; 2) sorting of genetic variation by natural selection. It represents a classic Darwinian framework in which natural selection is considered the creative force that causes adaptation (Gould 1982), and genes are assumed to be able to respond to selection indefinitely. Recently however, with the emergence of the field of Evo-Devo, this standard view of evolution has received much criticism (Pigliucci 2007; Pigliucci 2009; Laland et al. 2014). Because natural selection does not directly operate on genes, rather it is the traits translated from the genomic blueprint that ultimately determine the fitness of an organism. Moreover, natural selection operates within the context of existing variation, such that both the direction and intensity of natural selection could be altered by the origination of novel phenotypes. Therefore, understanding the processes underlies the production of phenotypic variation is of crucial importance towards a more comprehensive theory of evolution.

The diversification of craniofacial morphology has played a key role during vertebrate evolution. Adaptive variation in craniofacial structure facilitates specialization to

different food sources and habitats, which in turn contributes to niche partitioning and speciation. In fact, it has been argued that most of the morphological and functional divergence between vertebrates can be found in the craniofacial region (Gans & Northcutt 1983), which reflects adaptations to a wide variety of environments. It is thus not surprising that myriad studies have investigated patterns of craniofacial divergence in various animals, including (but not limited to) dogs (Drake & Klingenberg 2010; Schoenebeck et al. 2012), bats (Dumont et al. 2012), birds (Abzhanov et al. 2004; Abzhanov et al. 2006; Brugmann et al. 2010) and cichlids (Albertson et al. 2003a; Albertson et al. 2003b; Roberts et al. 2011). Although recent efforts have started to associate variation in trophic morphology with differences in gene expression (Abzhanov et al. 2004; Abzhanov et al. 2006; Wu et al. 2004; Wu et al. 2006; Albertson et al. 2005), the causative loci that underlie these differences remain largely unknown, especially in terms of complex and functionally relevant patterns of craniofacial divergence.

The explosive radiation of East African cichlids has produced a large degree of variation in craniofacial morphology (Kocher 2004; Cooper et al. 2010), providing an excellent system to study the genetic and developmental mechanisms that promote such variation. It has been shown that the diversification of trophic morphology among Lake Malawi cichlids is also correlated with specialized modes of feeding and resource partitioning and has likely contributed to their rapid speciation (Kocher 2004; Cooper et al. 2010). Because craniofacial structure arises from a complex and dynamic developmental program with both pleiotropic and modular effects (Helms & Schneider 2003), the expectation is that it should evolve via continuous fine-tuning steps. In accordance with

this prediction, it has been previously demonstrated that morphological differences between closely related cichlid genera are the result of directional selection on numerous genetic loci of small to moderate effect (Albertson et al. 2003b; Albertson et al. 2005). These studies identified numerous quantitative trait loci (QTL) for craniofacial morphology segregating in the F2 hybrid progeny of the genera *Labeotropheus* and *Maylandia* (Albertson et al. 2003a; Albertson et al. 2005). Although *Labeotropheus* and *Maylandia* are closely related rock-dwelling cichlid genera, they are divergent in craniofacial morphology and microhabitat utilization (Albertson & Kocher 2001; Cooper et al. 2010). *Labeotropheus* is a specialist algal scraper with robust jaws adapted for biting, whereas *Maylandia zebra* is a generalist with gracile jaws better adapted for suction feeding (Figure 1.1A & B). These two genera represent opposite ends of the benthic/limnetic eco-morphological continuum that characterizes East African cichlid radiations (Cooper et al. 2010) as well as many other notable divergences among teleosts at both the population and species level (Walker 1997; Adams & Huntingford 2002; Parsons & Robinson 2006; Riopel et al. 2008; Cooper & Westneat 2009). Identifying the molecular genetic basis for these eco-morphologic shifts therefore has the potential to inform a more comprehensive understanding of teleost diversity in general.

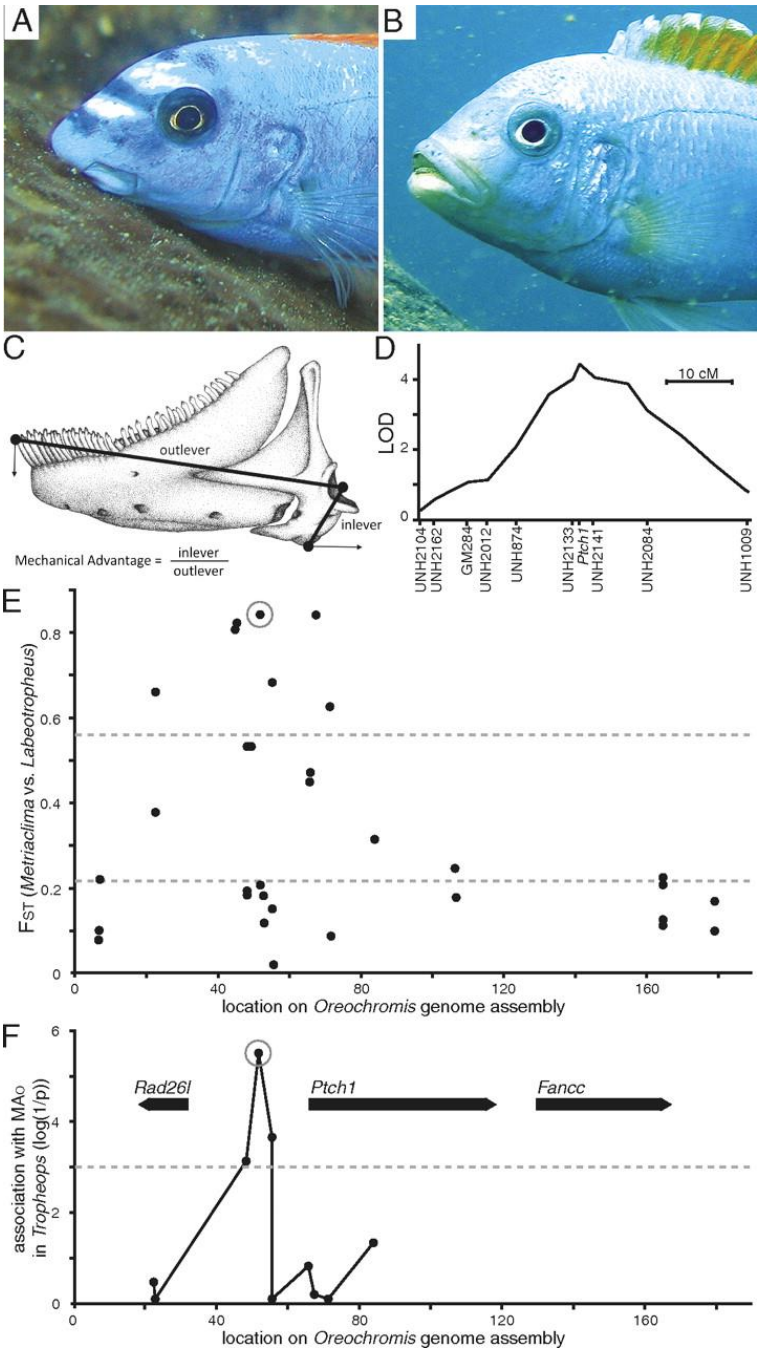

Figure 1.1. *Ptch1* locus characterization in families, genera, and populations. Craniofacial appearance of (A) *Labeotropheus trewavasae* (image courtesy of Justin Marshall) and (B) *Maylandia mbenjii*.(C) Lower jaw phenotype measures; RA and inlever length is equivalent. (D) QTL mapping interval for MA_O on cichlid LG12. (E) Population differentiation (FST) between *Labeotropheus* and *Maylandia* (n = 24 each) for SNPs at the *ptch1* locus. Dashed lines indicate two experimental measures of mean FST; the lower line from global comparison of *Labeotropheus* vs. *Maylandia* across many populations (20), and the upper line from comparisons of randomized *Labeotropheus* and *Maylandia* population pairs from distinct sites (48). (F) Significance of association between SNPs at the *ptch1* locus and MA_O in the genus *Tropheops* (Wald test, n = 59); dashed line indicates a P value of 0.001. Genes in the region annotated with bold arrows. The SNP used to indicate long and short alleles of *ptch1* is circled in E and F. From Reade B. Roberts et al. PNAS 2011;108:13194-13199

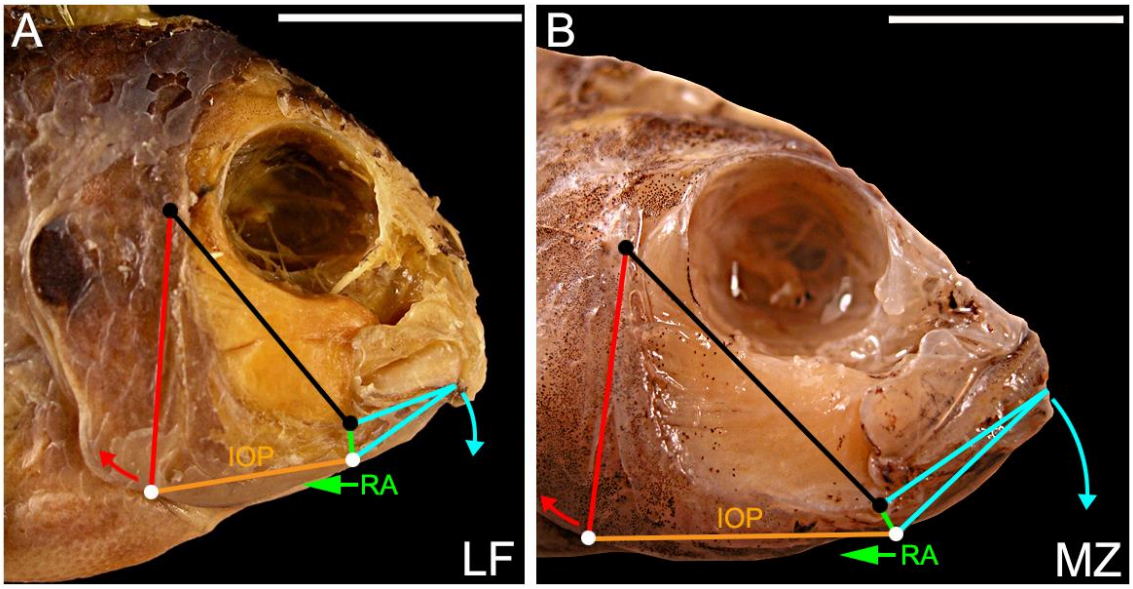

Figure 1.2. The opercular four-bar linkage system in LF and MZ. (A)LF is an algae scraper, which has a relatively longer RA and shorter IOP that results in slower jaw rotation. (B) MZ is a suction feeder that has a relatively shorter RA and longer IOP, which leads to faster jaw rotation. The black bar represents the fixed link, which extends from the opercle–neurocranium joint posteriorly to the mandible–quadrate joint anteriorly. The red bar is the input link, which extends from the opercle–neurocranium joint dorsally to the posterior most edge of the IOP bone ventrally. The orange bar (labeled IOP) is the coupler link, which extends from the posterior edge of the IOP bone to the insertion of the IOP ligament onto the ventral tip of the RA. The green bar (RA) is the output link, which extends from the mandible– quadrate joint to the ventral tip of the RA. The blue bars represent the length of the lower jaw from themandible–quadrate joint and the RA. Black circles represent fixed joints, whereas white circles are mobile joints. Arrowheads represent the direction of movement during jaw opening. From Yinan Hu, and R. Craig Albertson PNAS 2014;111:8530-8534

A recent genome scan study identified single nucleotide polymorphisms (SNPs) exhibiting unusually high differentiation (FST) between *Labeotropheus* and *Maylandia* (Loh et al. 2008). The high FST of these SNPs suggests they may be linked to genetic loci associated with evolutionary divergence between the two genera. Roberts et al. (Roberts et al. 2011) summarized the overlap between these genomic locations of high FST SNPs and previously identified QTL (Albertson et al. 2003b; Albertson et al. 2005), and used them as a starting point to identify the specific genes contributing to morphological divergence between the genera. With additional data from a third genus Tropheops, Roberts et al. hypothesized that genetic variation in the cis-regulatory region of the *ptch1* gene, which codes the receptor protein patched-1 for the Hedgehog pathway, mediates variation in the relative lengths of the retroarticular process (RA) of the mandible (Figure 1.1C-F, Roberts et al. 2011).

In this chapter, I provide developmental evidence to support this hypothesis, and further show that *ptch1* is contributing to additional variation beyond RA in the craniofacial skeleton. Specifically, I show that allelic variation in *ptch1* is associated with variation in the shape of both the retroarticular process (RA) of the mandible and the interopercle (IOP) bone. Together these two bones contribute to a complex functional system, the opercular 4-bar linkage chain (Figure 1.2), which is necessary for proper jaw opening in teleosts (Durie & Turingan 2004). The action of this 4-bar system is powered by the levator opercula, a muscle that originates on the skull and inserts along the dorsal aspect of the operculum. As it contracts, it rotates the operculum (input link) posterodorsally. Then, through a ligamentous connection, the interopercle serves as a coupler link that

transmits the posterior motion to the RA, which is effectively the output link of this system that directly opens the lower jaw. Variation in the relative length of either the RA or IOP is predicted to significantly affect the kinematics of the system (McCarthy & Soh 2011). Thus, the RA and IOP represent functionally integrated elements in the teleost skull. I show further that RA and IOP dimensions co-vary across multiple Lake Malawi cichlid species. Finally, I provide evidence that this co-variation may be maintained by both genetic and epigenetic mechanisms. In all I propose that the Hedgehog signaling pathway has played a critical role in promoting the functional divergence among cichlid species.

1.2 Materials and methods

1.2.1 Cichlid maintenance.

Cichlid species were collected from Lake Malawi, and reared in 40-gallon glass aquaria, at 28.5°C ±1°C on a 14 hour light/10 hour dark cycle. All larvae used for this project were F1 or F2 derived from wild-caught stock, and obtained by natural matings. Embryos were extracted from mouthbrooding females between 3-4 days post fertilization (stages 10-14), and incubated in 1 liter glass beakers with ~900mL of system water plus 2-3 drops of methylene blue at 28.5°C ±1°C. An aeration stone was placed at the bottom of the flask to provide enough air to keep the embryos vigorously swirling at the bottom of the flask. Embryo medium was changed every 2 days. Cichlid staging was according to (Fujimura & Okada 2007).

1.2.2 *In situ* hybridization.

Whole-mount *in situ* hybridization (WISH) was performed as previously described (Albertson et al. 2005). Embryos used for the reported experiments were raised, staged, fixed, and processed in parallel. Sense and antisense *ptch1* riboprobes were made from cichlid clones (sequence identical for LF, accession no. JN037690, and MZ, accession no. JN037691), corresponding to exons 1–7 and 7–17. These yielded identical WISH results; data derived from the exons 1–7 riboprobe are reported. Accession numbers for *gli1* and *col1a1* probes are JN037689 and JN116727, respectively. A *col10a1* riboprobe was made directly from cichlid cDNA using primers that contained T3 (sense) and T7 (antisense) RNA polymerase binding sequences: Col10a1_T3F1 CATTAACCCTCACTAAAGGGAACAGGAGCACCAGGTAAAAGC; Col10a1_T7R1 TA- ATACGACTCACTATAGGGAGAAGGACCTGGGAGACCAT. Polymerase recognition sequences are underlined. To facilitate probe penetration, alkaline hydrolysis was used to fragment probes to ≈500 bp. A solution of 20 mL RNA probe, 12 mL H_2O, 4 mL 0.4M sodium bicarbonate, and 4 mL 0.6M sodium carbonate was incubated at 60 °C for a period based on the following: time (min) = (starting kb − desired kb)/(0.11 × starting kb × desired kb).

1.2.3 QTL mapping.

I photographed and measured the length and width of the IOP in 114 F2 individuals derived from a cross between LF and MZ as described in (Albertson et al. 2003a; Albertson et al. 2003b). The calculated length-width ratio was used for QTL mapping, which was done in R using Multiple-QTL Mapping routines described in (Arends et al.

2010). Genome-wide significant threshold ($\alpha = 0.05$) was calculated by permutation tests with 1,000 repeats.

1.2.4 Cyclopamine treatment.

LF larvae (stage 17) from the same brood were divided into three treatment groups, cyclopamine treatment (LF CyA), ethanol control (LF EtOH), and untreated control (LF), with the same amount of larval fish water. In the cyclopamine treatment group, cyclopamine stock solution (10mM cyclopamine in ethanol) was added to reach a final concentration of 50 μM, based on (Fraser et al. 2008). The same volume of ethanol or larval fish water was added to the ethanol control and untreated control group respectively. Animals were treated for 6 hours in the dark at 28.5°C, and then washed with larval fish water several times before returning to standard culture flasks. At stage 25 (12 dpf), they were euthanized and stained with alizarin red and alcian blue for bone and cartilage (Walker & Kimmel 2007), then imaged with a Leica DFC450 C digital microscope camera mounted to a Leica M165 FC microscope. An MZ brood was stained and imaged with the same procedure for comparison. Measurements of bone development were taken from images with ImageJ 1.47.

1.2.5 Digital modeling of the opercular 4-bar linkage system.

Models were built in GeoGebra (http://www.geogebra.org/cms/en/). Lateral images of LF and MZ were imported as background to locate joint positions in default state (mouth closed). During simulations of mouth opening, the input link (opercle) was rotated posteriorly until the coupler link (IOP) and output link (RA) were aligned, which

prevents further rotation of the input link. The rotation of the input link was done stepwise with increments of 0.5°. At each increment, the corresponding output link rotation was recorded (ΔO), which was measured as the change in the angle between the output link and the fixed link. The KT ratio was then calculated at each increment as the output link rotation (ΔO) divided by the input link rotation (0.5°). When simulating *ptch1* induced phenotypic changes, I increased the length of coupler link (IOP) and decreased the length of output link (RA) from the LF model by 10%, 15% and 20% (e.g., model "*ptch1* 10%" is a LF model with 10% longer IOP and 10% shorter RA). These three models were chosen because they roughly approximate the magnitude of QTL effects of *ptch1* on IOP (17%) and RA (11%) shapes.

1.2.6 Monitoring gaping frequency.

Fish larvae were transferred to a small petri dish with ~10mL system water, and then allowed a 10min acclimation period before placed under a Leica M165 FC microscope. Gapes were counted real-time by looking at individual larva under the scope with a stopwatch. Disrupted observations (e.g. larva escaped field of view) were not recorded such that only continuous observations of more than 60 gapes were included in subsequent analyses.

1.2.7 Manipulation of gaping frequency.

MZ larvae (6dpf) from a single brood were divided into two groups: 1) Control group where individual larva was kept in large containers with ~150 mL of system water; 2) Experiment group where individual larva was kept in small containers with ~12mL of

system water. Water is replaced twice a day. The restriction of water/space appears to increase the frequency of gaping, though it might also introduce unexpected environmental variations.

1.2.8 IOP Surgery.

I anaesthetized stage 17 LF larvae from the same brood with tricaine at 0.2mg/mL according to (Neiffer & Stamper 2009), and the interopercle-mandibular ligament (IOPL) on the right side was cut with extra-fine forceps. Larvae were transferred into fresh larval fish water immediately after surgery to recover before returning to standard culture flasks. For sham surgeries, an incision of similar size was made to the tissue just anterior to the RA where no ligaments or skeletal elements were present. Control larvae were exposed to tricaine for approximately the same period of time but no surgery was performed. All larvae were allowed to develop for an additional four days to stage 23 (10dpf) and then euthanized and prepared for measurements (cleared and stained as above).

1.3 Results and discussion

1.3.1 Differential *ptch1* expression surrounding the retroarticular and interopercle immediately precedes differential bone development.

The signatures of genetic divergence in *ptch1* is immediately upstream of the coding region (Roberts et al. 2011), which suggests adaptation occurred via modulations in cis-regulatory elements. To explore potential roles for *ptch1* and Hedgehog signaling during cichlid craniofacial bone development, I examined the expression of *ptch1*, *gli1*, a

downstream target of the Hedgehog pathway, and two osteogenic markers, *col1a1* and *col10a1* via *in situ* hybridization in two cichlid species, *Labeotropheus fuelleborni* (LF) and *Maylandia zebra* (MZ) (Figure 1.3; Figure 1.4A-F; Figure 1.5). Dimensionality of the lower jaw is determined early, and in comparisons of LF and MZ differences in the shape of the lower jaw precursor (Meckel's cartilage) are evident as early as 5 days post-fertilization (dpf), stage 17-18 (Albertson et al. 2005; Fujimura & Okada 2007). By the following day (stage 18-19) many of the bones that constitute the feeding apparatus have begun to condense, and at this early stage one can observe discrete nodes of *ptch1* expression in areas where bone development has or will be initiated (Figure 1.3B–D & 1.3F–H). Notably, species exhibit differences in *ptch1* expression that correlate with biting and suction feeding jaw morphologies. In the long RA species LF there is marked expression of *ptch1* surrounding the lower jaw at this stage, with nodes of robust expression in or adjacent to areas of skeletal differentiation, including the regions where the dentary and RA will form (Figure 1.3B & D). In contrast, levels of *ptch1* are much lower in the short RA species MZ in the same context (Figure 1.3F & H). Unlike expression at the developing lower jaw, levels of *ptch1* expression are similar between LF and MZ in the developing fin-ray elements of the tail (Figure 1.3C & G). Quantitative differences in gene expression is then verified by q-PCR and pixel density analysis for both *ptch1* and *gli1* (Roberts et al. 2011).

Additionally, considerable overlap between *ptch1* and *col1a1* expression posterior to the RA is also observed (Figure 1.4A-F; Figure 1.5). Specifically, *ptch1* and *gli1* are broadly expressed in the hyoid region of the skull, surrounding the interopercle-mandibular

ligament (Figure 1.4C-D; Figure 1.5A-B). Within this ligament, *col1a1* is expressed in the anterior region (Figure 1.5C), while *col10a1* is expressed in the posterior region (Figure 1.4E-F; Figure 1.5D), indicating the onset of IOP bone deposition. Immediately after this stage of differential Hh expression, patterns of *col10a1* expression also differ between these two species. Compared to MZ, LF has a relatively wider and shorter expression domain of *col10a1* in the IOP (Figure 1.4E-F; Table 1.1), as well as an expanded expression domain at the base of the RA process (asterisk, Figure 1.4E-F). For the IOP, differences in *col10a1* gene expression predict differences in IOP shape across multiple stages of larval and juvenile development (Figure 1.4E-L; Table 1.1). Thus, different IOP shapes observed in adult fish (Figure 1.4M-N) can be traced to differential gene expression at the earliest stages of IOP bone development.

The IOP is a specialized sesamoid bone that is not present in basal fish groups (Lauder & Liem 1983). Shared among halecostome fishes, the IOP provides an novel biomechanical pathway of lower jaw depression, and is thought to be an evolutionary innovation that promotes the versatility of mouth opening mechanisms (Lauder 1980; Lauder 1982). Since *col1a1* expression within this ligament is located in the same region where *ptch1* is differentially expressed between LF and MZ (Roberts et al. 2011), I hypothesized that in addition to RA, the development of species-specific IOP shape might also be regulated by *ptch1*/Hedgehog signaling.

Age	Mean width/length ratio of IOP (±S.E.)		p value
	LF	MZ	
6 dpf*	0.152 ± 0.012	0.120 ± 0.005	p = 0.040
9 dpf	0.157 ± 0.016	0.023 ± 0.004	p < 0.001
12 dpf	0.243 ± 0.005	0.185 ± 0.008	p < 0.001
26 dpf	0.315 ± 0.003	0.265 ± 0.007	p < 0.001
adult	0.405 ± 0.007	0.312 ± 0.007	p < 0.001

Table 1.1. Width/length ratio of the IOP at different stages in LF and MZ. * At this stage the bone deposition in the IOP has just started and cannot be visuallized by alizerin red staining, so I measured the expression domain of Col10a1 instead. From Yinan Hu, and R. Craig Albertson PNAS 2014;111:8530-8534

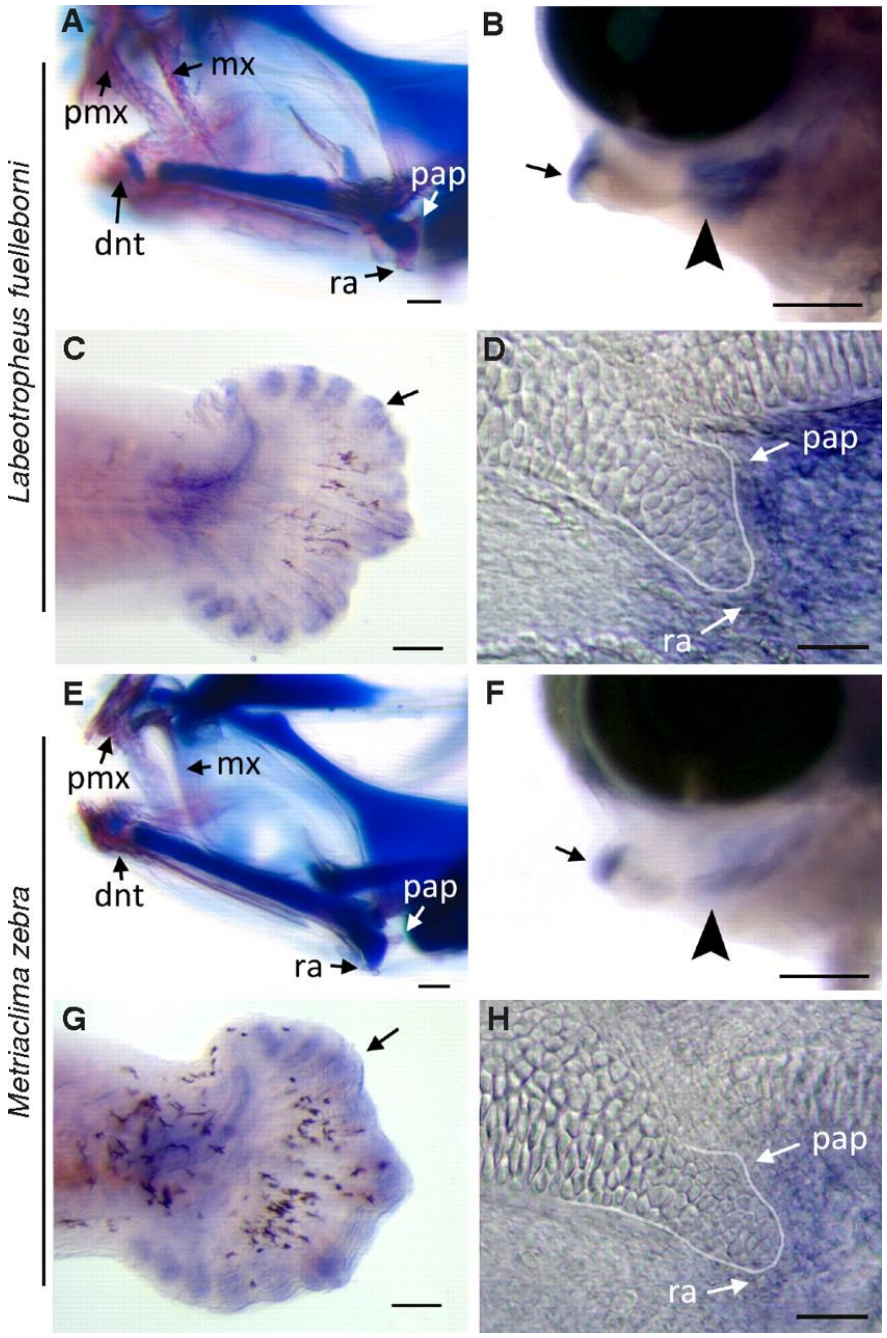

Figure 1.3. Interspecific differences in *ptch1* expression. Craniofacial outcomes in (A) LF and (E) MZ larvae at 13 dpf; LF larvae exhibit accelerated bone (pink) development compared with MZ; cartilage stains blue. *ptch1 in situ* labeling in representative 6-dpf (stage 17-18) (B–D) LF and (F–H) MZ larvae: (B and F) Lateral whole-mount view of lower jaw with nodes of *ptch1* expression, particularly in mesenchymal cells at the distal (arrow) and proximal (arrowhead) ends of the lower jaw precursor where the dentary and RA process will form, respectively. (C and G) *Ptch1* labeling is qualitatively similar in developing fin-ray elements of tail (arrows). (D and H) Flatmount preparation of the jaw joint in lateral view, showing the cartilaginous precursor of the RA process (outlined) relative to node of *ptch1* expression. dnt, dentary; mx, maxilla; pap, posterior articulation process; pmx, premaxilla. (Scale bars, 200 μm in A, B, E, and F; 100 μm in C and G; and 10 μm in D and H.) From Reade B. Roberts et al. PNAS 2011;108:13194-13199

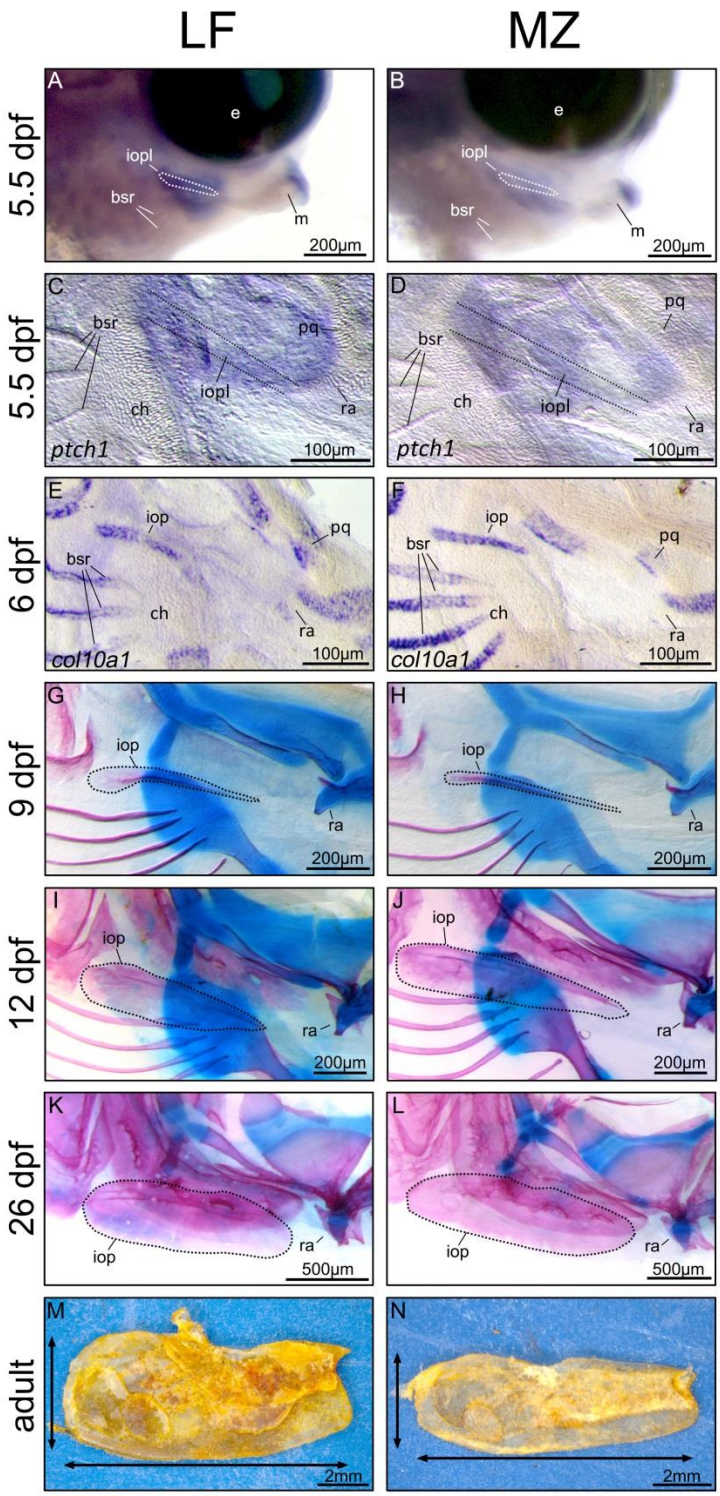

Figure 1.4. Differential expression of *ptch1* in the pharyngeal skeleton precedes differential development of the IOP in LF and MZ. (A–F) *In situ* hybridization results showing gene expression at stage 17–18 (5.5–6 dpf). (A and B) Lateral view of the whole mount. (C–F) Flat mount preparations of the pharyngeal skeleton. (G–L) Flat mount of cleared and stained (alizarin red and Alcian blue) pharyngeal skeletons. Dashed line outlines the IOP. (M and N) Dissected adult IOP. bsr, branchiostegal rays; ch, ceratohyal; e, eye; iopl, interopercular–mandibular ligament; m, Meckel's cartilage; pq, palatoquadrate; ra, retroarticular. From Yinan Hu, and R. Craig Albertson PNAS 2014;111:8530-8534

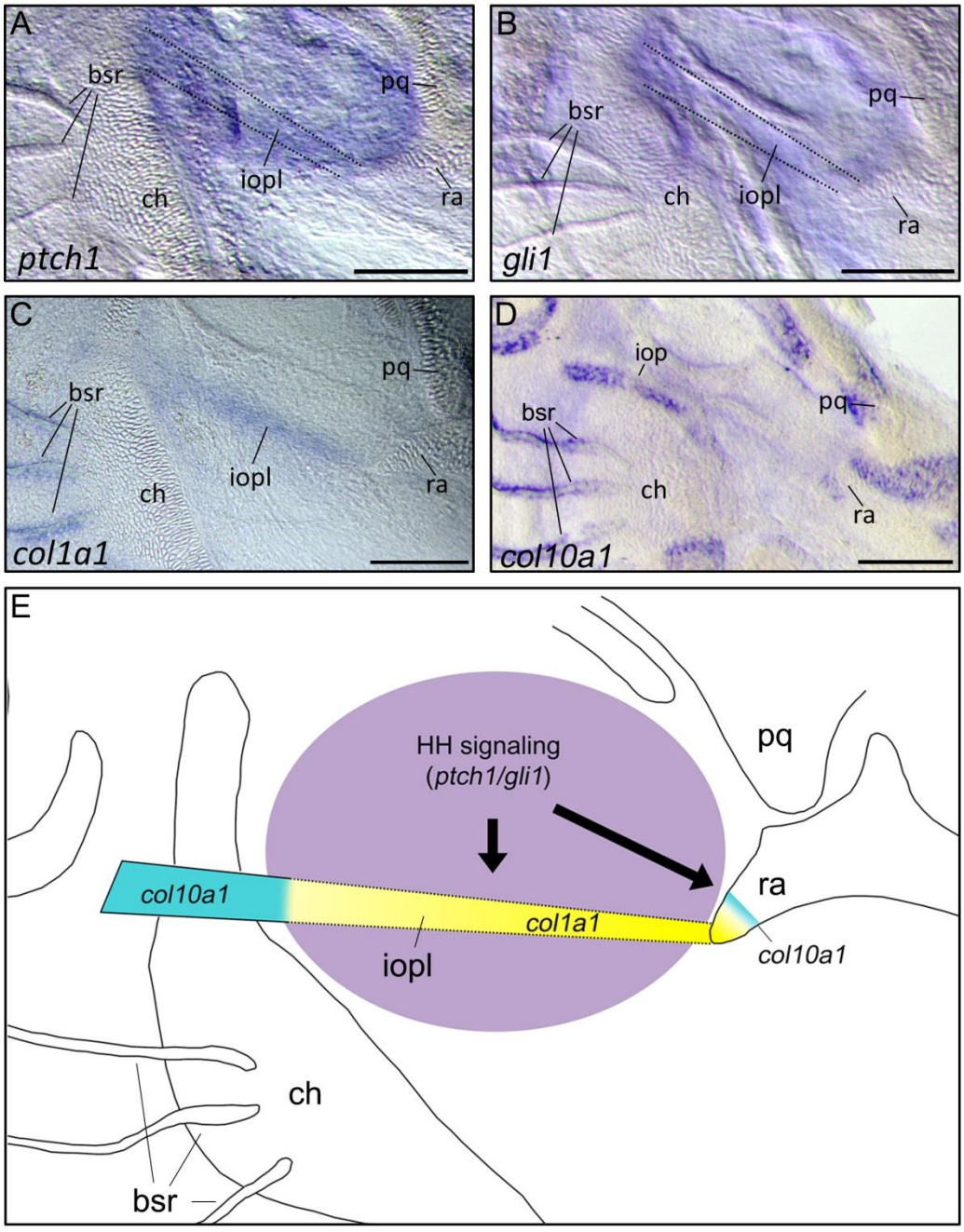

Figure 1.5. Hypothesized model of Hedgehog signaling pathway mediates both RA and IOP development. A-D: *In situ* hybridization results showing the expression of *ptch1*, *gli1*, *col1a1* and *col10a1* in LF at stage 17-18. *Ptch1* is the receptor of the Hedgehog pathway; *Gli1* is a downstream target of the Hedgehog pathway; *Col1a1* is a marker for early osteoblast differentiation; col10a1 is a marker for late osteoblast differentiation. E: An illustration of the hypothesis depicting the expression of all four genes around the IOP and RA. bsr: branchiostegal rays; ch: ceratohyal; iop: interopercle; iopl: interopercla-mandibular ligament; pq: palatoquadrate; ra: retroarticular. Scale bar, 100 μm. From Yinan Hu, and R. Craig Albertson PNAS 2014;111:8530-8534

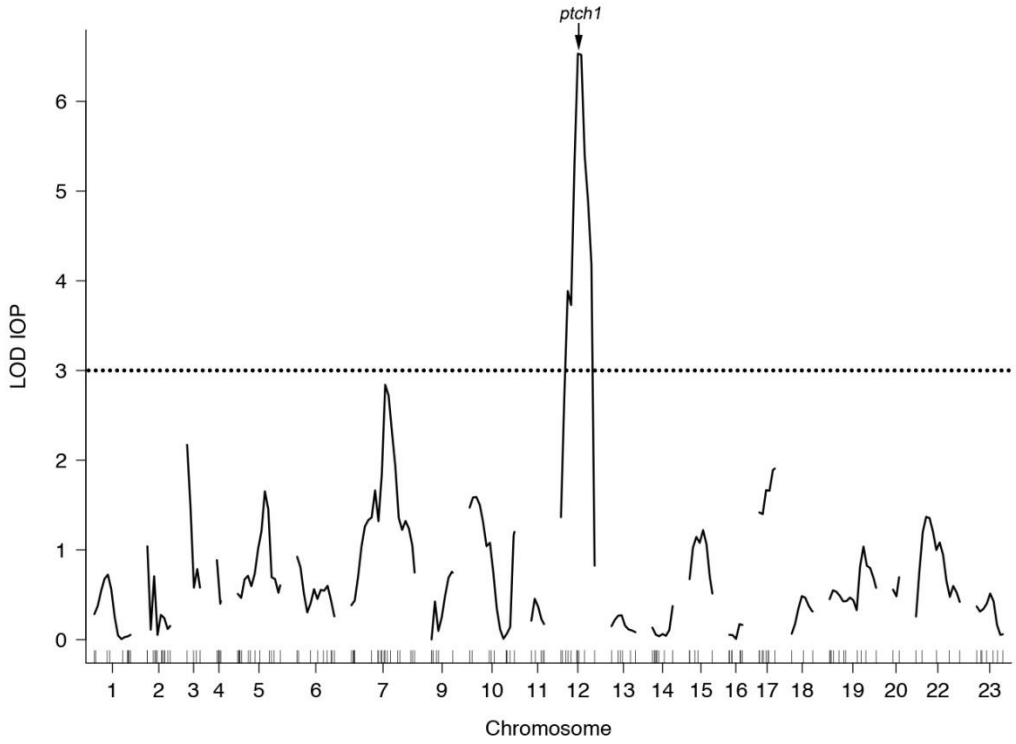

Figure 1.6. QTL mapping results for IOP shape. Showing QTL intervals associated with the width/length ratio of IOP across the cichlid genome. Dotted line indicates genome-wide significance threshold (α=0.05). From Yinan Hu, and R. Craig Albertson PNAS 2014;111:8530-8534

QTL model	Linkage group	Position of LOD peak (cM)	Bayes credible interval of QTL peak (cM)	Nearest marker	LOD	PVE (%)	Coeficient of additive effect	Coefficient of dominance effect
IOP W/L ratio	12	25	18 - 42	MET3573	6.245	17	0.0595	0.0005

Table 1.2. QTL mapping results for width/length ratio of IOP. PVE, percent variance explained. From Yinan Hu, and R. Craig Albertson PNAS 2014;111:8530-8534

1.3.2 A single QTL for IOP shape maps to *ptch1*.

As a first step toward testing this hypothesis about IOP, I conducted a QTL analysis in an F2 population derived from a cross between LF and MZ. A single QTL interval on linkage group (LG) 12 that affected the width/length ratio of the interopercle was detected (Figure 1.6). And as predicted, the QTL peak was located squarely on the *ptch1* locus, and the allelic effects were consistent with the interspecific variation observed between parental species: inheritance of the ancestral (LF) *ptch1* allele was associated with the development of a relatively wider and shorter IOP, whereas the derived (MZ) allele was associated with a relatively narrower and longer IOP. The QTL exhibited an additive mode of inheritance (Table 1.2), and accounted for 17% of the phenotypic variance in the F2 population.

1.3.3 Chemical manipulation of the Hedgehog signaling pathway recapitulates natural interspecific variation in RA and IOP shape.

The gene expression data was consistent with recent work demonstrating a role for Hedgehog signaling in bone development (Abzhanov et al. 2007; Hammond & Schulte-Merker 2009), and genetic mapping on IOP shape indicates *ptch1* is also involved in morphological variation in the IOP. Therefore, I predicted that modulation of the Hedgehog pathway can lead to variation in both RA and IOP shape. To test this prediction I treated LF larvae with cyclopamine, an antagonist of Hedgehog pathway signaling (Chen et al. 2002), at a critical stage of craniofacial bone development and *ptch1* expression (stage 17). During normal development, both *ptch1* and its downstream target *gli1* are expressed in areas adjacent to or coincident with the bone differentiation

marker *col1a1* (Figure 1.5A-B; Figure 1.7A-L). In treated larvae, I found that expression of both *ptch1* and *gli1* is dramatically and globally reduced (Figure 1.7P-W). I also found that bone development is delayed in areas where *ptch1* is normally expressed (Figure 1.7X-AA). Specifically, less *col1a1* expression was observed around the developing RA, whereas more cells were expressing *col1a1* around the branchiostegal rays and within the caudal fin (Figure 1.7Y–AA), suggesting that these structures were in a more undifferentiated state after cyclopamine treatment relative to control animals. Expression of *col1a1* around the dentary was relatively unaffected by cyclopamine treatment (Figure 1.7X); however, this is likely because development of this structure was well underway at the stage when animals were treated.

Overall, these patterns of expression were consistent with the phenotypic outcome of cyclopamine treatment. Specifically, I found that cyclopamine-treated larvae exhibit significantly reduced RA length (measured as MA_O), whereas the dentary and overall length of the lower jaw, which is determined primarily by outgrowth of Meckel's cartilage that occurs earlier than the stages examined here, remains roughly the same (Figure 1.8). In addition, I also found that treated LF larvae exhibited IOP width/length ratios that were statistically indistinguishable from those of MZ (Figure 1.9). Thus, in terms of gene expression patterns (Figure 1.7), relative bone development (Figure 1.7), MA_O (Figure 1.8), and IOP shape (Figure 1.9), cyclopamine-treated LF recapitulate a suction-feeding, MZ-like phenotype. Although the specific cellular mechanism of how *ptch1* affects RA and IOP development remains to be investigated, these results suggest that both RA and IOP shape is specifically mediated by the Hedgehog signaling pathway.

In addition, note that treated animals exhibited bifurcated expression of *col1a1* within the developing branchiostegal rays (asterisk in Figure 1.7Z), as well as aberrant expression within the dermal fin ray elements of the caudal fin (arrow in Figure 1.7AA). These patterns are also consistent with craniofacial defects after cyclopamine treatment, in which fusion of the branchiostegal rays and truncation of the caudal fin ray elements were observed (Figure 1.7AC-AD; Figure 1.9A). These data extend previously documented roles for Hedgehog signaling in dermal bone development (Abzhanov et al. 2007; Hammond & Schulte-Merker 2009) and suggest that this pathway plays an important role in polarizing dermal bone development along a proximal–distal axis. It is well established that Hedgehog signaling is critical for the proper patterning and polarization of several organs in various animal taxa (Krauss et al. 1993; Ingham & Fietz 1995; Koyama et al. 1996; Chuong et al. 2000; Tanaka et al. 2000; Harris et al. 2005), but here a similar role has been documented for bone development. The extent to which Hedgehog-mediated outgrowth of other dermal bones (e.g., RA) has influenced species-specific differences in craniofacial shape would be a fruitful area of future investigation.

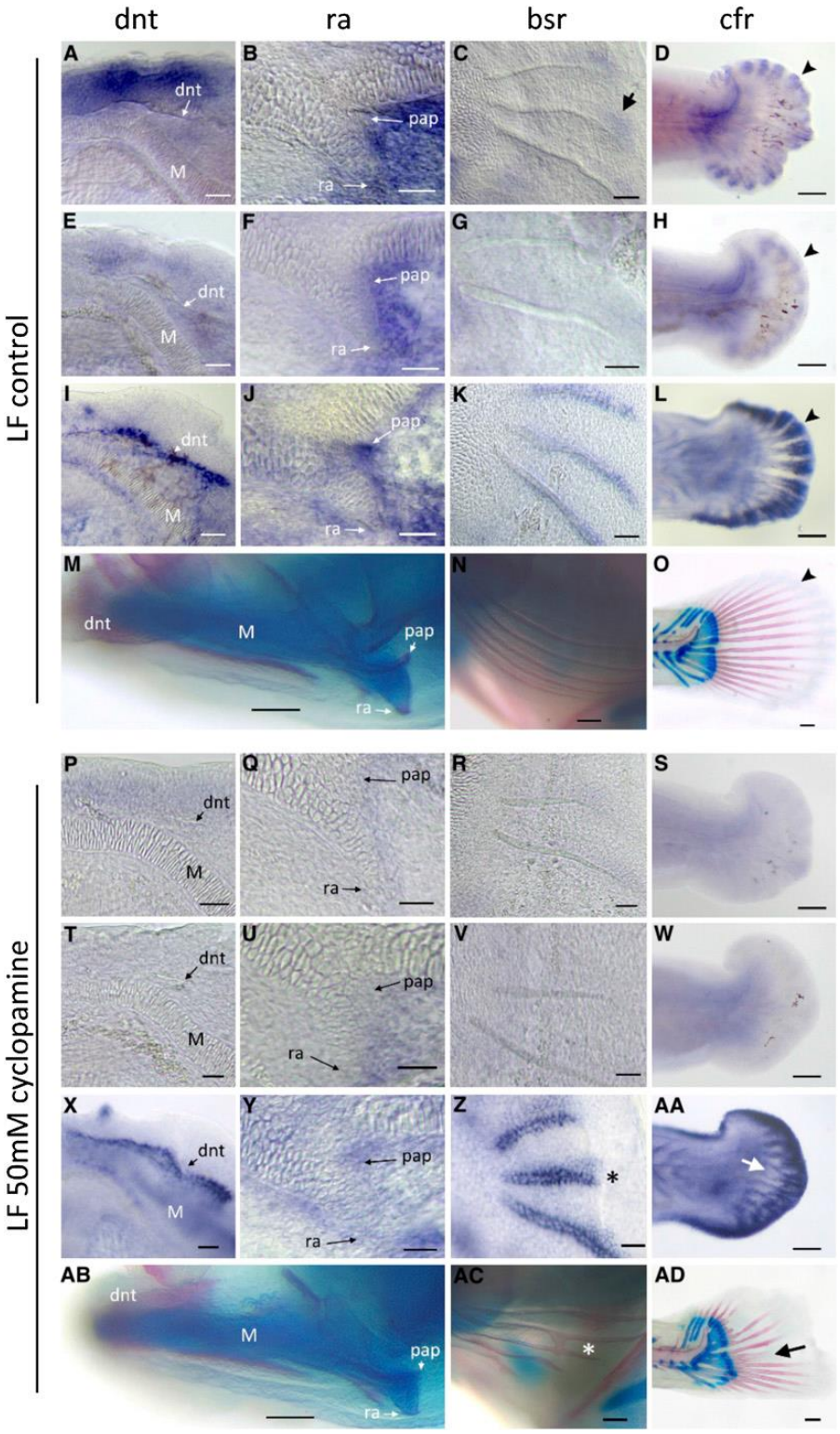

Figure 1.7. Hedgehog pathway is necessary for proper craniofacial bone development. Expression of the Hedgehog receptor *ptch1* (A–D), its downstream target *gli1* (E–H), and the bone differentiation marker *col1a1* (I–L) is shown in 6dpf (stage 12) *Labeotropheus fuelleborni* (LF) larvae. Co-localized expression was observed around the developing dentary (A, E, I), retroarticular (B, F, J), branchiostegal rays (C, G, K; note the discrete node of *ptch1* expression at the distal end of these bones in C, arrow; although *gli1* expression was not observed around these structures, G), and within the dermal fin ray elements of the

caudal fin (arrowheads D, H, and L). Mineralized structures are shown as a reference in older fish (12 dpf,M–O). Treatment with a Hedgehog pathway inhibitor resulted in the down-regulation of Hedgehog signaling and aberrant craniofacial bone development. LF larvae were treated with 50 μM of cyclopamine at 5.5 dpf (stage 11) for 6 h. Expression of *ptch1* (P-S) and its downstream target *gli1* (T–W) were drastically reduced. Although expression of the osteoblast differentiation marker *col1a1* was relatively unaffected in the dentary (X), its expression in other structures suggests an attenuation and/or delay in bone development. Specifically, *col1a1* expression was reduced around the retroarticular process (Y), whereas expanded expression was observed around the branchiostegal rays (Z) and within the caudal fin(AA), suggesting that these structures are in a more undifferentiated state relative to control animals. Also notice the bifurcated expression of *col1a1* in the branchiostegal rays of cyclopamine-treated animals (asterisk in Z), as well as disorganized expression within the developing caudal fin ray elements (arrow in AA). The phenotypic outcome of this treatment is consistent with altered patterns of gene expression. Although the dentary is relatively unaffected in cyclopamine-treated animals, the length of the retroarticular process is reduced in treated animals (AB). In addition, the branchiostegal rays are bifurcated and fused in treated animal (AC), and dermal fin ray elements are dramatically reduced in the caudal fin(AD). bsr, branchiostegal rays; cfr, caudal fin rays; dnt, dentary; M, Meckel's cartilage; pap, posterior articulation process; ra, retroarticular. (Scale bars, 10 μmin A–C, E–G, I–K, P–R, T–V, and X–Z; and 100 μmin D, H, L–O, S, W, and AA–AD.) From Reade B. Roberts et al. PNAS 2011;108:13194-13199

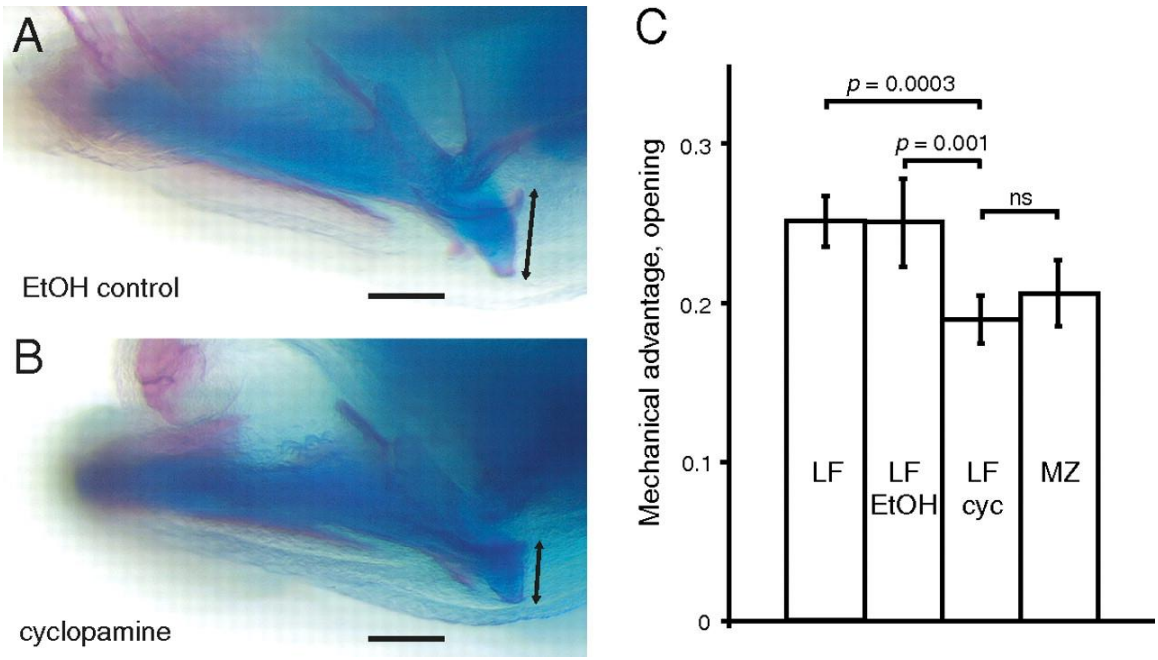

Figure 1.8. Treatment of biting species larvae with a Hedgehog pathway inhibitor recapitulates a suction-feeding jaw phenotype. LF larvae were treated with (A) 0.5% ethanol (EtOH control, n =7) or (B)50 μM cyclopamine (cyc, n = 10) for 6 h at stage 12; RA length measured at 12 dpf (black arrow in A and B). (C) Relative to the length of the lower jaw (measured as the distance between the center of the jaw joint and the tip of the dentary), RA length (measured as the distance from the posterior tip of the posterior articulation process to the ventral tip of the retroarticular) was significantly reduced in cyclopamine treatment group compared with the control LF group but was not significantly different from MZ control larvae (n = 7). Larvae treated with ethanol were in- distinguishable from untreated siblings (n =6). P values, one-way ANOVA. (Scale bar, 100 μm.) From Reade B. Roberts et al. PNAS 2011;108:13194-13199

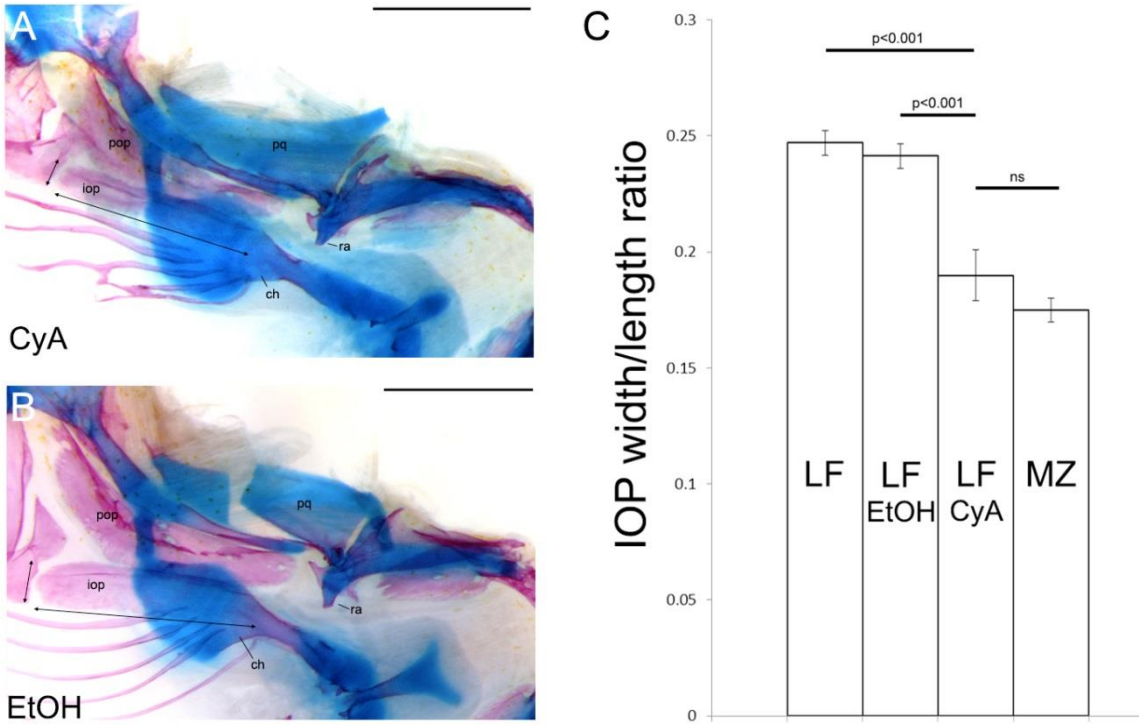

Figure 1.9. Cyclopamine treated LF larvae recapitulates an MZ-like IOP phenotype. LF larvae were treated with either 50 μM cyclopamine (CyA, n = 7) or 0.5% ethanol (EtOH control, n = 7) for 6 hours at stage 17 (6 dpf). IOP length and width (black arrows) measured at stage 25 (12 dpf). A-B: flat mount of cleared and stained pharyngeal skeletons. C: Barplot showing the width/length ratio of IOP was significantly reduced in cyclopamine treated group compared with the EtOH control group, but was not significantly different from untreated MZ larvae (n = 8). Larvae treated with ethanol were not distinguishable from untreated siblings (n = 5). ch: ceratohyal; iop: interopercle; pop: preopercle; pq: palatoquadrate; ra: retroarticular; P values, Tukey's HSD. Scale bar, 200 μm. From Yinan Hu, and R. Craig Albertson PNAS 2014;111:8530-8534

With these data, I propose that natural variation in both IOP shape and RA length between LF and MZ is caused, at least in part, by two alternatively fixed *ptch1* alleles. The functional difference between these two alleles results in different transcript levels being produced in an area of the skull where both the IOP and RA develop (Figure 1.3; Figure 1.4A-F; Figure 1.5; (Roberts et al. 2011)). The LF allele is associated with elevated *ptch1* expression, a relatively long RA, and a relatively wider/shorter IOP. The MZ allele is associated with reduced *ptch1* expression, a shorter RA, and narrower/longer IOP.

1.3.4 Co-variation of interopercle and jaw shape among natural populations of cichlids.

The above results suggest that a single locus alters two functionally related bones in the cichlid skull. I next set out to assess whether this genetic association is reflected in patterns of variation among natural populations of cichlids. To this end I measured IOP and RA dimensions in several closely related wild caught cichlid species from Lake Malawi that exhibit a range of foraging modes. Besides LF and MZ, an additional four species from the *Tropheops* species complex were included. Whereas LF and MZ represent opposite ends of the biting-suction feeding continuum among mbuna, *Tropheops* species were chosen that represent various points along this continuum. I show that patterns of variation in the relative length of the RA, measured as the mechanical advantage of jaw opening (MA_O), precisely matches that of the width/length ratio of the IOP in these six species (Figure 1.10). Moreover, patterns of co-variation are consistent with the frequency of *ptch1* alleles across species. In LF, the ancestral allele is fixed, and they show the highest MA_O and width/length ratio of the IOP. In MZ, the

derived allele is fixed, and they show the lowest MA_O and width/length ratio of IOP. Among *Tropheops* species, the two *ptch1* alleles are still segregating, and they show a range of MA_O and IOP ratios. Notably, *Tropheops* species fixed for the derived allele exhibit MA_O and IOP phenotypes that match those of MZ, whereas species with higher frequencies of the ancestral allele have phenotypes closer to LF (Figure 1.10). These results support the assertion that the Hedgehog signaling pathway contributes to ongoing trophic adaptations in Malawi cichlids (Roberts et al. 2011).

Co-variation, or integration, of traits is believed to be a major factor that determines evolvability (Klingenberg 2008). In particular, coordinated changes in multiple traits can promote patterns of variability that, when aligned with the vector of selection, can result in rapid evolutionary responses (Schluter 1996). As two out of three movable links in the opercular 4-bar system, the RA and IOP represent functionally integrated elements of the teleost head. Here I show that these elements are also integrated at the evolutionary (i.e., the co-variation across species), developmental, and genetic levels. This widespread integration may provide greater insights to the outstanding diversity in cichlid trophic morphology: instead of two independent mutations, these fish can generate morphological changes in two bones that operate in a common function via a single mutation that affects the Hedgehog signaling pathway (e.g. *ptch1*).

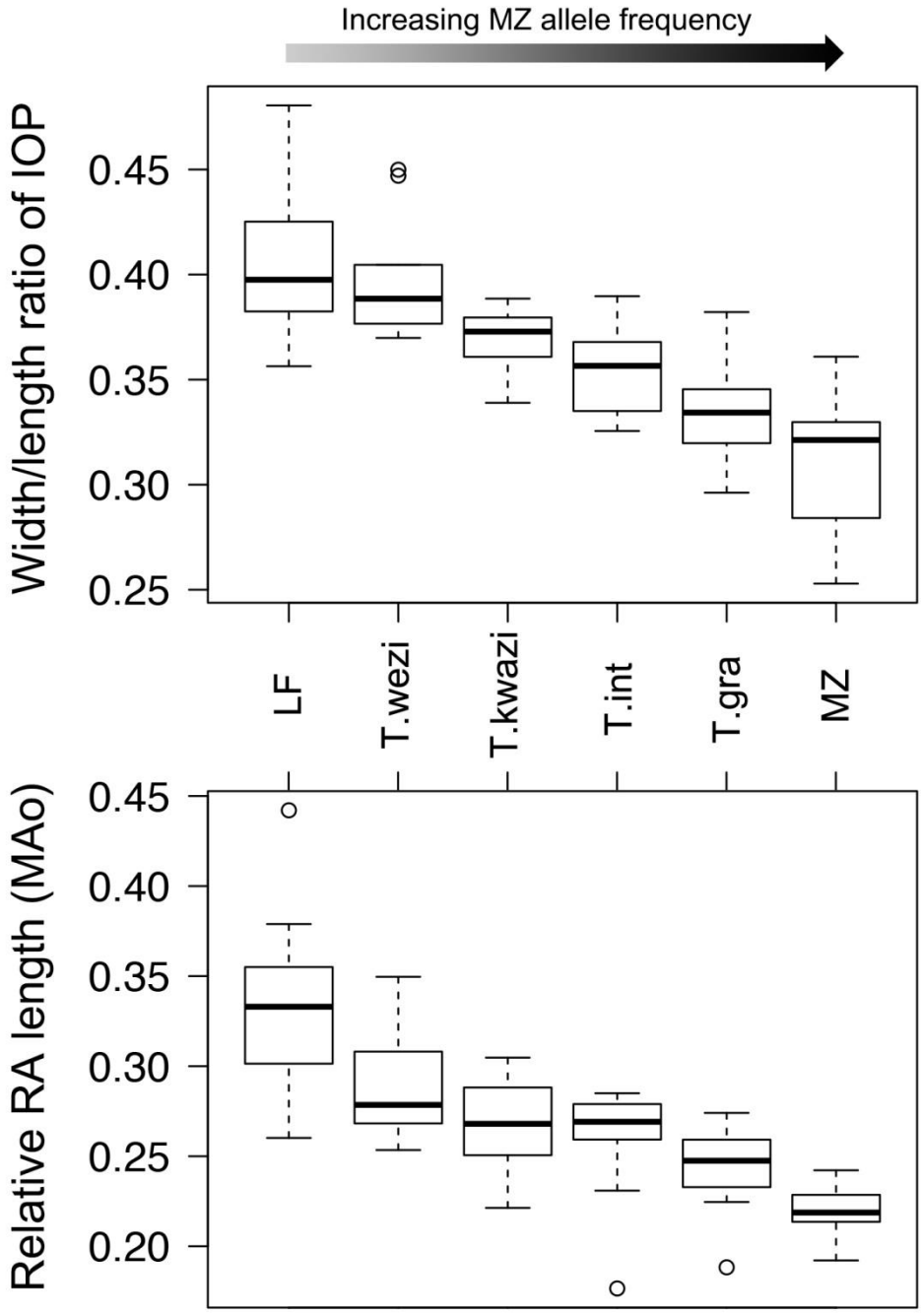

Figure 1.10. Co-variation of MA_O and width/length ratio of IOP across species. LF, *Labeotropheus fuelleborni*, 0% MZ (derived) *ptch1* allele; T.wezi, *Tropheops sp.* from chinyamwezi, 27% MZ *ptch1* allele; T.kwazi, *Tropheops sp.* from chinyankwazi, 59% MZ *ptch1* allele; T.int, *Tropheops intermedius*, 100% MZ *ptch1* allele; T.gra, *Tropheops gracilior*, 100% MZ *ptch1* allele; MZ, *Maylandia zebra*, 100% MZ *ptch1* allele. From Yinan Hu, and R. Craig Albertson PNAS 2014;111:8530-8534

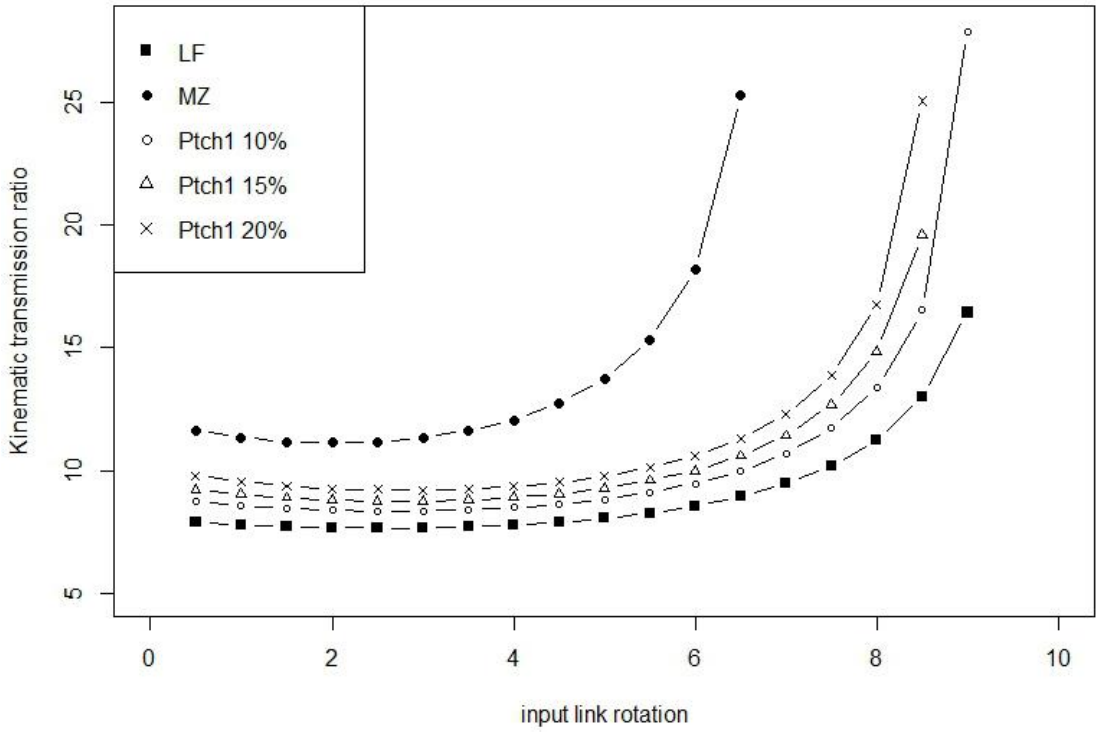

Figure 1.11. Kinematic transmission ratio (KT) during jaw opening in digital models of the opercular 4-bar linkage system. X axis: the rotation of the input link from starting position. Y axis: KT. LF: model that represents the LF morphology; MZ: model that represents the MZ morphology; *Ptch1* 10%: modified LF model with 10% longer IOP and 10% shorter RA; *Ptch1* 15%: modified LF model with 15% longer IOP and 15% shorter RA; *Ptch1* 20%: modified LF model with 20% longer IOP and 20% shorter RA. From Yinan Hu, and R. Craig Albertson PNAS 2014;111:8530-8534

1.3.5 *Ptch1* induced changes to the RA and IOP are predicted to influence the mechanics of the opercular 4-bar linkage system.

To investigate the potential biomechanical outcome of Hedgehog-induced shape variation in the IOP and RA, I built digital models and simulated the movement of the opercular 4-bar linkage system under different scenarios (Figure 1.11) and monitored changes in kinematic transmission ratio (KT) during jaw opening. First, I simulated the model with parameters that depicted the parental phenotypes, and show that during jaw opening, KT is higher in the suction-feeding species (MZ) than the biting species (LF). This is consistent with the general observation that suction-feeding species usually possess 4-bar systems that are capable of faster jaw movements, i.e. higher KT (Westneat 1994; Westneat 1995; Wainwright 2004). Next, I manipulated parameters in the LF model (i.e., representing the ancestral condition) to simulate *ptch1*-mediated phenotypic changes in the IOP and RA toward a more MZ-like condition (i.e., representing the derived condition). Note here I was using the IOP as a proxy for the coupler link since it contributes to ~85% of the length of the coupler link in both species. As expected, I found that with a progressively longer IOP, and progressively shorter RA, KT shifts away from the LF/ancestral model towards the MZ model (Figure 1.11).

1.3.6 Is covariation of IOP and RA shape due to genetic or epigenetic mechanisms?

I have demonstrated that IOP and RA shapes (i) are affected by a single QTL that maps to *ptch1,* (ii) are similarly affected by cyclopamine treatment at the same stage of cichlid craniofacial development, and (iii) co-vary across closely related and ecologically similar cichlid species (Hu & Albertson 2014). These observations are consistent with a role for

genetic pleiotropy in mediating both IOP and RA dimensions. However, given the functional linkage between these two elements, which is evident at early stages of cichlid craniofacial development (i.e., when the RA and IOP first mineralize), it is also possible that the shape of one of these elements is influenced by the shape of the other via epigenetic processes (e.g. mechanically induced bone deposition). To address this question, I tested the hypothesis that during jaw opening, the repeated pulling of the IOP on the RA (via the interopercle-mandibulary ligament, IOPL) will stimulate bone deposition on the RA. Key to the credibility of this hypothesis is the observation that cichlid larvae start to repeatedly open and close their jaws soon after the lower jaw forms (~stage 17-18, 6dpf). This gaping behavior begins as the RA and IOP first develop, and occurs at a surprisingly high frequency that ranges from 160 ~280 times/min. It is unlikely that this behavior is due solely to respiration and/or ionoregulation needs, because at this early stage gill filaments are still developing, and the skin alone is sufficient for gas and ion exchange (Rombough 2002). Interestingly, there also appears to be species-specific differences in gaping frequency: on average, LF larvae gapes faster than MZ, and a third species *Tropheops tropheops* (TT) that has an intermediate bone morphology, gapes at an intermediate frequency (Figure 1.12). This trend coincides with differences in RA length, therefore I predict that, as an alternative (or complement) to respiration and ionoregulation, this repeated opening of the lower jaw via contraction of the interopercle-mandibular ligament will introduce mechanical stress upon the RA, thereby inducing bone deposition on this element (Nomura & Takano-Yamamoto 2000; Thompson et al. 2012).

To test this hypothesis, I manipulated the gaping frequency in MZ larvae by restricting them in a smaller container with much less water, which leads to a higher gaping frequency (Figure 1.13). Note that this approach may also induce unnoticed physiological response besides the behavioral change in gaping (e.g. higher levels of stress hormones), so the results should be interpreted with caution. Nevertheless, MZ larvae kept in small containers started to gape significantly faster at 8dpf, and when essayed for phenotype on 10dpf, they developed a longer RA compared to the control group (Figure 1.14; $p<0.002$, two tail t-test), while the overall developmental progress remained the same (based on standard length and caudal fin skeleton). Since frequent gaping likely produces a larger amount of mechanical stimulus, this observation is consistent with my hypothesis that variation in RA development could be induced epigenetically.

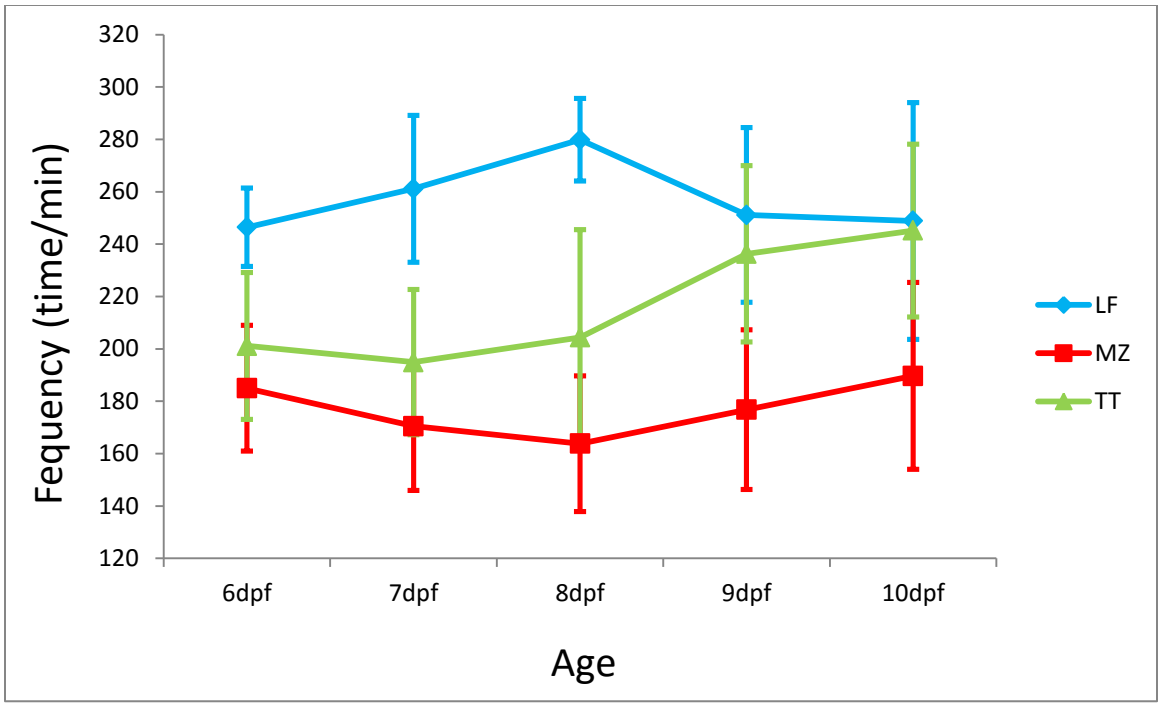

Figure 1.12. Gaping frequency of cichlid larvae over ontogeny.

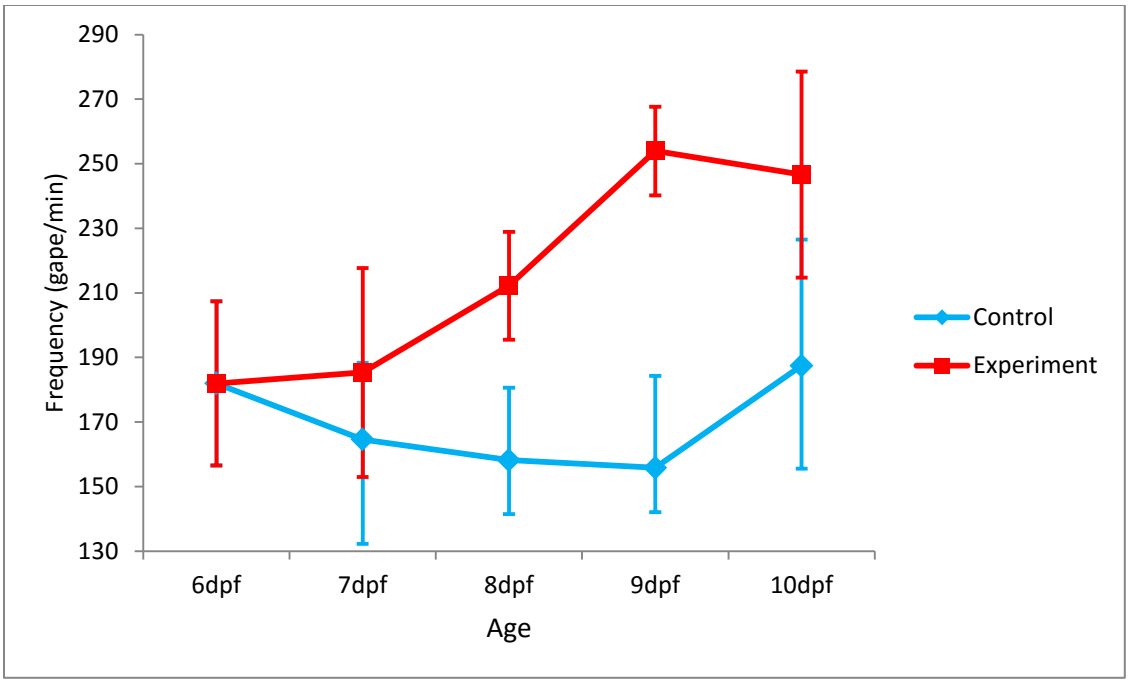

Figure 1.13. MZ larvae restricted in smaller container showed higher gaping frequency. Control: MZ larvae kept in large flask/beaker with ~150mL fish water. Experiment: MZ larvae kept in small beaker with ~12mL fish water.

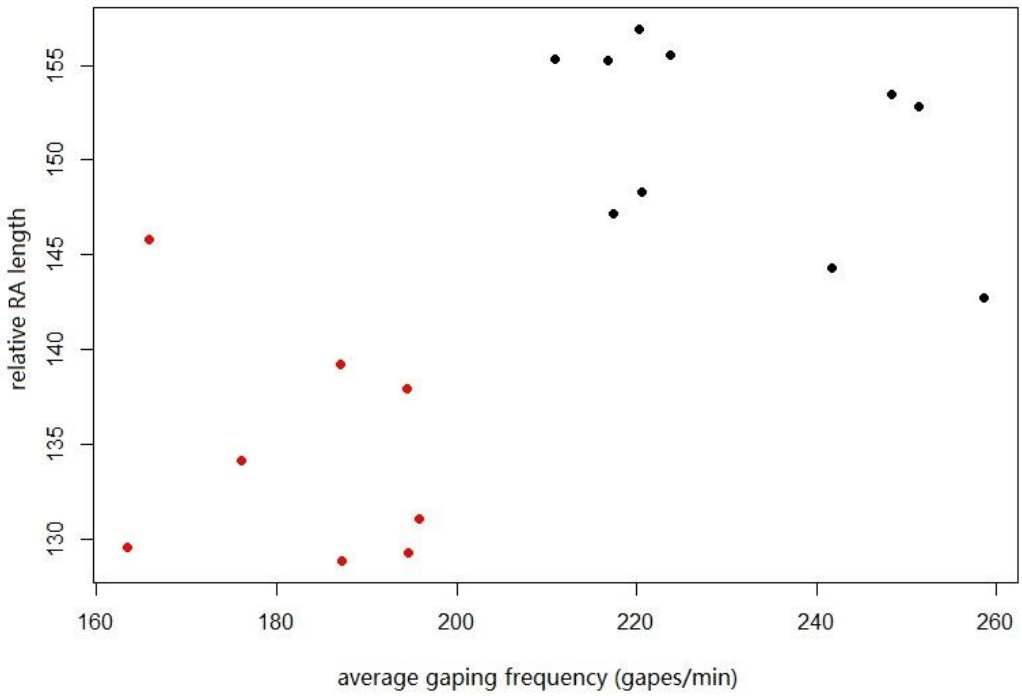

Figure 1.14. Variation in gaping frequency is associated with relative RA length in MZ. x-axis: average gaping frequency of each individual larva from 6dpf to 10dpf. y-axis: relative RA length measured on 10dpf. Red dots: individuals kept in flask/large beakers. Black dots: individuals kept in small beakers.

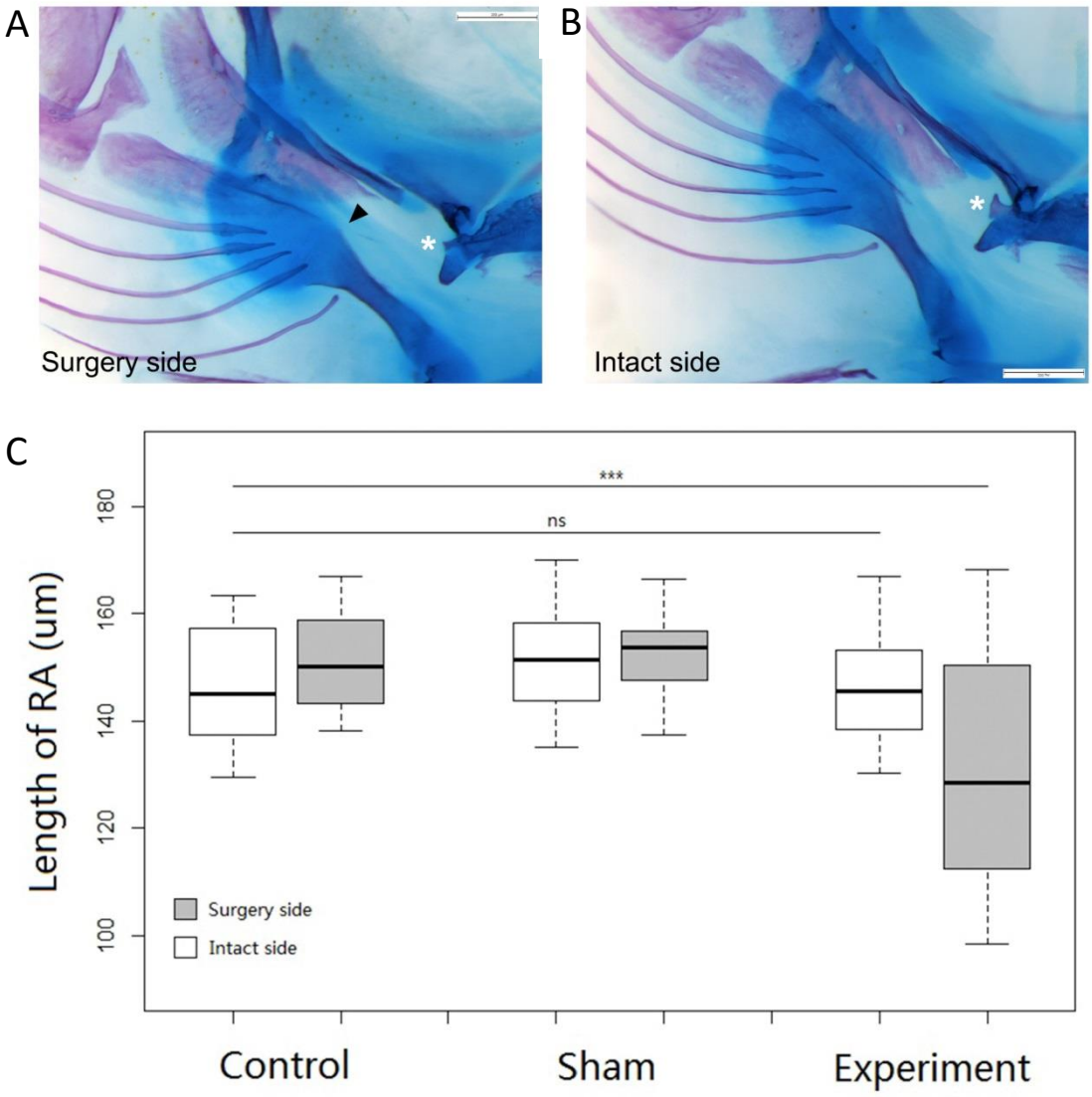

Figure 1.15. Surgical manipulation of the IOP influences bone development in the RA. Top panel: flat mount of cleared and stained pharyngeal skeletons of one representative individual from the experiment group showing the surgery side (A) and intact side (B). Black arrowhead points to a breakage in the IOP resulted from the surgery. Asterisks: RA. Bottom panel: boxplot summarizing the result of the IOP surgery experiment. In the experiment group (n = 26), the IOPL was cut; in the sham group (n = 23), a cut with the same size was made in tissue just anterior of RA; in the control group (n = 14), fish larvae were exposed to the same dose of anesthetic for the same time period, but no surgery was performed. All surgery was performed in stage 17 (early 6dpf) LF larvae on the right side only. IOP and RA shapes were measured at stage 23 (10dpf). ***: statistical significance ($p<0.05$), Tukey's HSD.

Next, in order to more explicitly test this hypothesis, I surgically cut the interopercle-mandibular ligament on the right side of LF larvae at stage 17 (6dpf), while the left side was left intact. Fish were allowed to recover for 4 days, at which point they were assessed for differences in bone morphology. My prediction was that the RA on the surgical side should receive less mechanical stress and thus would become shorter than the RA on the intact side. To account for generalized effects of surgery (e.g., inflammation), I performed sham surgeries where incisions of a similar size were made to tissue immediately anterior to the RA. Notably, my surgical manipulation of the IOPL resulted in a breakage in the IOP (Figure 1.15A, arrowhead), which likely attenuates the amount of force that can be transmitted from the IOPL to the RA. Moreover, and consistent with my prediction, surgical manipulation of the IOP resulted in changes in the RA (Figure 1.15C). Specifically, I found that the RA on the surgical side was significantly shorter compared to the control side ($p<0.001$, Tukey's HSD), which suggests that the observed effect is due to differential forces being propagated to different sides of the fish. It is also notable that the effects on RA development after surgical manipulation of the IOP were observed in less than 4 days. If extrapolated over months of development and differential mechanical stress, it is certainly plausible that genetic effects specific to IOP could be propagated to the RA. Thus, the phenotypic integration between IOP and RA could be due to either the pleiotropic effects of *ptch1*/Hedgehog signaling shared by these two bones, or epigenetic factors that influence bone development via mechanical stress. The data presented in this chapter certainly leave open the possibility that both may be playing a role in mediating the co-variation between IOP and RA on a broader evolutionary scale (i.e. across species). They also underscore the importance of

developmental processes when studying the mechanisms that underlie the manifestation of adaptive phenotypic variation.

1.4 Conclusion

One of the key questions in evolutionary studies is how genetic variation translates into ecomorphological adaptation, and ultimately fitness (Dalziel et al. 2009; Irschick et al. 2013; Parsons & Albertson 2013). Here I present empirical evidence that variation at a single locus affects multiple components in a dynamic mechanical system characterized by several distinct moving elements. I show that in cichlids, *ptch1* mediates morphological variation in both the IOP and RA (integrated genetically). I also demonstrate that the mode of action of this affect can be traced to early stages of bone development – e.g., expression patterns of the osteogenic marker *col10a1* differ between LF and MZ. Ultimately, these molecular and anatomical differences translate to variation in the mechanical properties of the opercular 4-bar linkage model (integrated functionally), a complex functional system that is predicted to play important roles in the ecological divergence among closely related teleost species (Westneat 1994; Westneat 1995; Wainwright 2004). I show further that the coordinated morphological evolution between IOP and RA across multiple cichlid species (integrated evolutionarily) may be the result of both genetic and epigenetic mechanisms (integrated developmentally). In all, this work offers an integrative view on how adaptive radiations can occur at the genetic, developmental and functional levels.

CHAPTER II

A NEW METHOD TO EVALUATE PHENOTYPIC INTEGRATION ON THE INDIVIDUAL LEVEL

2.1 Introduction

How traits co-vary with each other can impose constraints that may have profound effects on the outcome of evolution. The study of phenotypic integration provides an empirical approach to study such trait interactions, typically through measures of covariance (Pavlicev et al. 2009; Parsons et al. 2012). While important roles for integration have long been recognized in evolutionary biology (Mayr 1954; Olson & Miller 1958), it has received increased attention in recent years as researchers have begun to focus more explicitly on the origins of phenotypic variation (Pigliucci 2004; Hallgrimsson & Hall 2005; Klingenberg 2008). Specifically, integration is thought to be a major factor determining evolvability (i.e., the propensity to produce adaptive variation) by concentrating variation along certain dimensions that ultimately biases the direction of evolution (Klingenberg 2008). The dimensions that explain the greatest amount of variation are determined by the pattern of integration, which refers to the structure of covariation among sets of traits (e.g., Figure 2.1B&C). They are predicted to influence the rate of adaptation toward a fitness optimum, with faster rates associated with patterns that are more in line with the axis of selection (i.e. evolutionary line of least resistance. Schluter 1996). The magnitude of integration refers to the strength of correlation among traits. A low degree of correlation (Figure 2.1A) might be associated with greater opportunity for a phenotype to evolve in a number of directions, whereas higher degrees

of correlation should limit the potential direction of evolutionary change to fewer dimensions (Figure 2.1B&C). While the effects of integration may degrade over time (Schluter 1996), there is evidence that integration has influenced evolution over extended periods of time (Marroig & Cheverud 2005). Thus, a largely open question in the field is the degree to which integration itself may evolve over time. A key step in addressing this question is to garner a better understanding of the genetic basis of phenotypic integration.

Recent progress along these lines has been made through the analysis of phenotypic integration in laboratory mutants, which has demonstrated that both the magnitude and pattern of integration can be influenced through the manipulation of candidate genes with known function and developmental roles (Hallgrímsson et al. 2009). However, the extent to which genes identified via mutagenesis contribute to variation in integration within and among natural populations remains unclear. As a complement, I believe that the application of forward genetics (i.e., genetic mapping) has the potential to greatly facilitate our ability to understand the genetic basis and evolution of phenotypic integration. One obstacle to this approach is the ability to measure phenotypic integration at the individual-level. Traditionally, integration is assessed within populations since such studies require measuring patterns and magnitudes of covariation in groups. Recently, however, Parsons et al. (2012) adopted a jackknife approach that allowed inter-individual variation in integration *patterns* to be evaluated and genetically mapped for the cichlid mandible (Parsons et al. 2012). Here I extend this approach to assess the genetic basis of the *magnitude* of phenotypic integration.

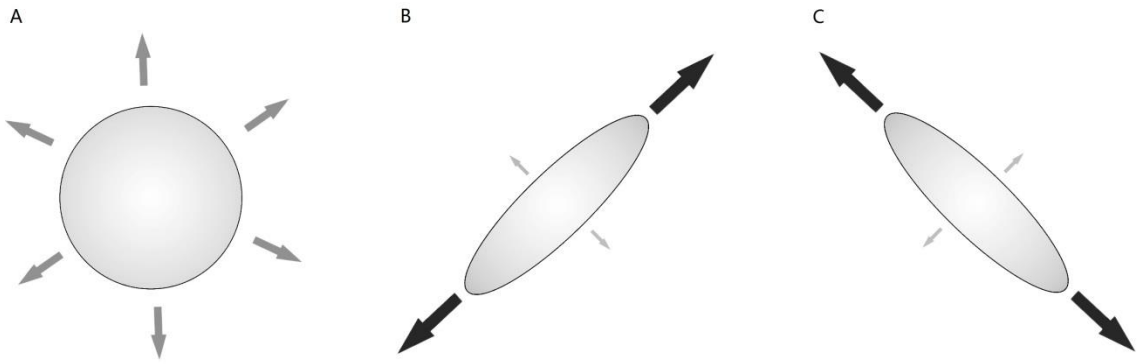

Figure 2.1. How integration influences evolution. Adapted from Klingen- berg 2010. **A)** Representation of a population with a low magnitude of integration among a set of traits. Variation is evenly distributed in phenotypic space, and thus this trait complex can respond with equal efficiency to selection in any direction (maximized opportunity). **B)** A representative population with a high magnitude of integration among the same set of traits. In this example, there is a high degree of correlation among traits, and so variation is concentrated along one dimension in phenotypic space. Compared to a, this trait complex is predicted to evolve faster if the direction of selection is parallel to the primary axis of phenotypic variation, but it won't be able to respond as quickly if the axis of selection is perpendicular to that of phenotypic variation. **C)** A population with a high magnitude of integration among the same set of traits, but with a different pattern of integration than b. Variation is concentrated along a different dimension in phenotypic space. From Yinan Hu et al. Evol Bio 2014;41:145-153.

The East African cichlids provide an excellent opportunity to study phenotypic integration and its influence on evolvability as these fishes demonstrate an outstanding capacity for rapid and repeated phenotypic diversification (Danley & Kocher 2001; Cooper et al. 2010; Parsons et al. 2011). Morphological variation in the cichlid feeding apparatus, which is predicted to affect mechanical properties and thus facilitate trophic adaptation, is a particularly important dimension of divergence among cichlid radiations (Cooper et al. 2010). The observation of dramatic yet highly stereotypical patterns of trophic divergence among cichlid lineages triggers the question of what role phenotypic integration has played during these radiation events. To begin to address this question, I compared integration magnitude between two Lake Malawi cichlid species that exhibit different degrees of eco-morphological specialization. Assuming that selection favors the coordination of traits during adaptation to a specialized niche (Rosas-Guerrero et al. 2011), my prediction was that, relative to the more generalized feeder, the specialized species should exhibit a more integrated phenotype. Using a new statistical approach I then measured and genetically mapped QTL related to the magnitude of integration in the mandible of an F2 population derived from these two species. I identified several regions of the genome as well as epistatic interactions that modulate mandibular integration, offering new insights into the genetic bases of integration in the cichlid mandible.

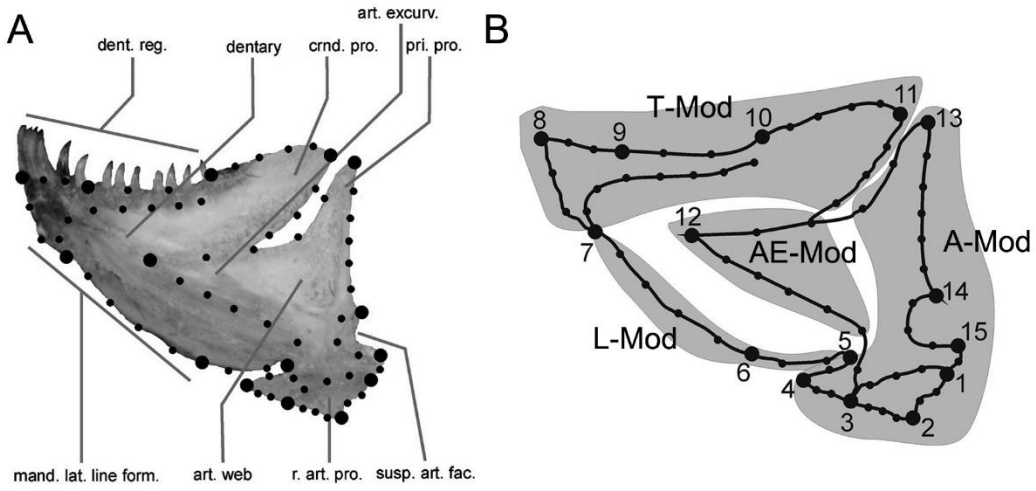

Figure 2.2. The left lateral view of the cichlid mandible showing the landmark positions and the pattern of integration in the F2 population. Adapted from Parsons et al. 2012. **A)** The anatomical regions of the mandible in a representative sample and the landmarks (large black circles) and semilandmarks (small black circles) collected for analysis. dent. reg. dentigerous region, crnd. pro. coronoid process, art. excurv. articular excurvation, pri. pro. primordial process, mand. lat. line. form. mandibular lateral line foramina, art. web articular web, r. art. pro. retroarticular process, susp. art. fac. suspensoriad articulation facet. **B**), Venn diagrams depicting individual modules in the mandible. T-Mod the tooth-bearing module, A-Mod the articular module, L-Mod the lateral line module, AE-Mod the articular extension module. From Yinan Hu et al. Evol Bio 2014;41:145-153.

2.2 Methods

I used wild-caught individuals from two Lake Malawi cichlid species, *Labeotropheus fuelleborni* (LF, n=25) and *Maylandia zebra* (MZ, n=25) and an F2 hybrid population (n=144) derived from crossing these two species (see Albertson et al. 2003a for details) in this study. LF is a phenotypically derived, ecologically specialized species with short, robust jaws for scraping algae from the rocky substrate (Albertson & Kocher 2001). Among the majority of East African cichlid species, LF occupies a novel region of craniofacial morphospace (Cooper et al. 2010). MZ on the other hand, exhibits a more generalized trophic phenotype with a relatively elongated craniofacial skeleton that it used to forage both from the substrate and the water column (Albertson & Kocher 2001; Cooper et al. 2010). Landmarks used for this analysis are shown in Figure 2.2. Landmark data was acquired as described in Parsons et al. 2012 and processed in R (version 2.15.1).

A covariance-based principal components analysis (PCA) was performed on partial warps scores. PC scores for PC1 were used to map the primary axis of shape variation, which describes relative differences in jaw height and length (Albertson & Kocher 2001; Albertson et al. 2003a; Albertson et al. 2005; Albertson et al. 2008). Magnitudes of integration were determined from eigenvalues which are scalar values that represent the amount of variation accounted for by each PC axis (Pavlicev et al. 2009). When the covariance (integration) among traits is high, the first few PC axes will account for much of the total variance. Correspondingly, these axes will present high eigenvalues relative to subsequent axes, and thus the variance among eigenvalues will be high. Alternatively, when the covariance among traits is low, the variance will be distributed more evenly

over many PC axes, and the variance among eigenvalues will be low. I took this approach to compare the magnitude of integration between LF and MZ at the population level using MorphInt (Peres-Neto 2005; MorphInt: available upon request from Peres-Neto. pedro@uqam.ca). Covariance matrices were used for the PCA, and confidence intervals (alpha=0.05) and associated P-value were calculated via bootstrapping the difference in eigenvalue variance 1000 times. I used Disparitybox6 to calculate "Foote disparity" as a measure of shape variances between the two groups (following Cooper et al. 2010).

In order to transform integration into a quantitative trait, I estimated each individual's contribution to the magnitude of integration at the population-level. This was achieved by calculating the variance of scaled eigenvalues (VSE) of the whole population (scaled eigenvalues provide estimates of the percent variance accounted for by each axis) and the VSE of the same population without a particular individual. The difference between these two VSE values was then assigned to that individual as its integration score. If VSE goes up after removal of an individual, it can be inferred that that individual detracted from the overall magnitude of integration within the population, and would result in a negative score. Alternatively, if VSE goes down, then the individual that was removed must have contributed to overall integration, and its integration score would be positive. Thus, this metric provides a relative assessment of the contribution of an individual to the integration magnitude of the whole population. This process was repeated for every individual in the population. Eigenvectors were determined from the entire F2 population and held constant to prevent axes rotation during the calculation. This step ensured that only magnitudes and not patterns of integration changed during the removal of each

individual. I performed the analysis on partial warp scores extracted from morphological data of the mandible. Integration metrics were derived from landmark datasets for the entire lower jaw, as well as subsets of the data which describe previously identified modules (see Figure 2.2 and Parsons et al. 2012) within the lower jaw. See appendix for the R script for this procedure.

QTL analyses were then conducted on PC1 scores and these newly generated integration scores using routines available in R and described in Broman and Sen (2009). Standard interval mapping was performed first, and significant QTLs were selected as potential cofactors that were then verified by backward elimination during subsequent Multiple-QTL Mapping (MQM) scans at default significance threshold of 0.02 (Arends et al. 2010). J-qtl (version 1.3.3) was used for two-QTL scans (epistatic interactions). I used Haley-Knott regression as scan method. Logarithm of the odds (LOD) scores for interaction were calculated as the LOD for the full model minus the LOD for the additive model and so were interpreted as evidence for interaction (Broman & Sen 2009). Genome-wide significant thresholds (α=0.05) for all QTL analyses were calculated by permutation tests with 1000 repeats.

QTL Model	Linkage group	Postion of LOD peak (cM)	Nearest marker	LOD*	PVE	Mean trait value for each genotype:		
						LF/LF	*LF/MZ*	*MZ/MZ*
MQM: Integration for Full lower jaw	19	20	GM634	3.82	7.65%	2.33E-06	-5.82E-07	-7.28E-07
MQM: Integration for Articular module (A-Mod)	2	20	UNH2135	4.13	5.40%	4.79E-06	6.63E-06	-4.52E-06
MQM: Integration for Tooth-bearing module (T-Mod)	9	0	UNH2063	3.43	8.11%	-3.03E-06	1.99E-06	-5.34E-06
MQM: PC1 for Full lower jaw	20	0	GM602	3.97	3.54%	-3.53E-03	-3.49E-03	4.63E-02
MQM: PC1 for Articular module (A-Mod)	20	0	GM602	4.78	5.06%	3.61E-03	3.32E-03	-3.32E-02

Table 2.1. Results of single QTL analysis. Grey shaded cells represent allelic effects that increase trait value in the F2. *All LOD scores are significant at the 0.95 level. PVE, percent variance explained by the QTL. From Yinan Hu et al. Evol Bio 2014;41:145-153.

QTL Model	Linkage group	Postion of Lod peak (CM)	Nearest marker	LOD*	PVE	Mean trait value for each genotypic combination:			
Epistasis: Full lower jaw	11	17.2	GM131a	7.439	28.50%	UNH2094	GM131a		
	6	0	UNH2094				*LF/LF*	*LF/MZ*	*MZ/MZ*
						LF/LF	-2.07E-07	-8.79E-07	-1.82E-06
						LF/MZ	-4.25E-07	2.57E-08	-3.17E-07
						MZ/MZ	7.00E-06	-6.20E-07	-1.54E-06
Epistasis: Articular module	10	20	UNH2169	8.68	14.40%	GM602	UNH2169		
	20	0	GM602				*LF/LF*	*LF/MZ*	*MZ/MZ*
						LF/LF	-3.97E-07	4.06E-06	-1.21E-06
						LF/MZ	4.99E-06	1.07E-06	-2.54E-06
						MZ/MZ	-4.30E-07	1.38E-05	6.22E-05

Table 2.2. Results of epistatic QTL analysis. Grey shaded cells represent allelic effects that increase trait value in the F2. *All LOD scores are significant at the 0.95 level. PVE, percent variance explained by the QTL. From Yinan Hu et al. Evol Bio 2014;41:145-153.

2.3 Results

According to expectations, the population-level comparison showed that LF, the phenotypically extreme species, had a significantly ($P<1*10^{-6}$) higher integration magnitude (0.001316) than MZ (0.001053). Note that LF analyzed here did have a higher Foote's disparity than MZ (not shown), which increases the statistical power for detecting integration in the LF population. While increased power does not necessarily guarantee a higher magnitude of integration, the result of my population level comparison should be interpreted with caution. Nevertheless, based on this result I predicted that alleles inherited from LF would contribute to higher magnitudes of integration in the F2 population.

Overall I identified three QTLs and two epistatic interactions that significantly affect the magnitudes of integration, and another QTL that influences the shape of the cichlid mandible (Table 2.1& 2.2). For the full lower jaw I detected one QTL on linkage group (LG) 19 where LF alleles had a recessive effect increasing integration magnitude. I also detected one epistatic interaction in which integration magnitude was increased when two MZ alleles on LG6 were paired with two LF alleles on LG11, whereas all other allelic combinations had similar integration magnitudes. Notably, the single-QTL on LG19 overlapped with a previously identified QTL for integration pattern (Parsons et al. 2012), suggesting a potential interaction between pattern and magnitude of integration. I also found one QTL on LG20 that influences the shape, represented by PC1 score here, of the full lower jaw.

Next, I analyzed integration magnitudes for previously identified modules within the lower jaw (Figure 2.2B). For the module that defines the posterior, or articular, region of the lower jaw (A-Mod), I identified one QTL on LG2 where LF alleles act to increase integration via a dominant mode of action. I also identified one interaction for this module between loci on LG10 and LG20. The homozygous MZ genotype at both loci increased integration magnitude. Notably, in my single QTL models the MZ/MZ genotype at each locus did act to increase integration magnitudes, but the effects were not significant. The same locus on LG20 contributes to shape variation in this module as well as the full lower jaw, suggesting a potential relationship between shape and integration. For the tooth-bearing module (T-Mod), I identified one QTL on LG9 where the heterozygous genotype increased integration magnitudes (i.e., overdominance). I was not able to detect any significant QTLs or interactions for neither the lateral line module (L-Mod) nor the articular extension module (AE-Mod).

2.4 Discussion

The Lake Malawi cichlid radiation event occurred over the past ~700,000 years and has resulted in more than 700 species (Danley & Kocher 2001; Turner et al. 2001), among which LF is one of the most phenotypically derived as it occupies a unique area of craniofacial morphological space (Cooper et al. 2010). It is also arguably one of the cosmopolitan cichlid species in the lake as it can be found at nearly every rocky shore (Ribbink et al. 1983). Interestingly, the ecological success of LF, in terms of abundance and geographical distribution, may have come at the expense of future diversification, as

it is one of the only two species within the genus *Labeotropheus* (Ribbink et al. 1983; Konings 2001). The genus *Maylandia,* on the other hand, contains many species that are relatively diverse in terms of ecology and morphology (Konings 2001; Streelman et al. 2007). Although fewer species of *Labeotropheus* does not necessarily mean they are less evolvable, these trends are consistent with the idea that LF may be constrained in a way that prevents further diversification. One hypothesis is that the extreme jaw shape of LF has evolved at the expense of evolvability: their mandibles are highly integrated which may have facilitated their adaptation to their current niche, presumably an evolutionary optimum, yet such high magnitudes of integration now serve as an evolutionary constraint that limits variability and further evolution. My population-level comparison of integration magnitude is consistent with this hypothesis. While a higher degree of integration is associated with eco-morphological specialization in LF, lower magnitudes of integration are associated with the more generalized trophic architecture of MZ. Here, lower magnitudes of integration may have facilitated the diversification in this group: variation is distributed relatively evenly in the morphological space and thus can respond to selection on multiple directions, i.e. divergent selection.

Differences in the magnitude of integration between LF and MZ at the population level led to the prediction that alleles from LF should increase integration. Two out of three QTLs identified in my single-QTL analysis were consistent with this prediction, but my genetic data also underscore the complexity and non-additive nature of this trait. To illustrate the complexity of the underlying mechanisms that produces phenotypic integration, Hallgrímsson proposed the Palimpsest Model (Hallgrímsson et al. 2009) in

which the final pattern of covariance is determined by multiple layers of developmental processes. In other words, each developmental process will generate different covariance patterns and the final output is the result of many such patterns superimposed upon each other. Since development is hierarchical, the effect of each covariance generating process may either reinforce or dilute subsequent processes, making it very difficult to decipher the mechanisms that underlie patterns and magnitudes of covariation observed in the adult structure. As a solution, Hallgrímsson proposed that a reverse genetic approach, such as the evaluation of chemically induced mutations in laboratory organisms, could provide an inroad into the molecular mechanisms that underlie integration.

My data support the idea that phenotypic integration has a complex genetic basis, but it also suggests that a classic forward genetic approach (e.g. genetic mapping) can be used to complement work in laboratory mutants to study the mechanisms that underlie phenotypic integration. Genetic mapping does not require prior knowledge about the developmental mechanisms that underlie a trait complex. Here I am using it as an unbiased scan through the genome for loci that predispose developmental systems to produce interactions among sets of traits. Moreover, loci identified via genetic mapping have the potential to decipher the Palimpsest in ways that are perhaps more concrete than the analysis of mutants. For one, integration QTLs represent the loci that are associated with actual (rather than potential) species divergence. In addition, understanding non-additive modes of inheritance of integration, including epistatic interactions, can provide insights into loci that may potentially be acting during multiple developmental processes. For example, the two epistatic loci identified in my analysis that by themselves only

slightly increase integration magnitudes in the articular module, but together contribute to a significant increase in integration, potentially represent two distinct layers of the Palimpsest (i.e. distinct developmental events). Testing this hypothesis will require narrowing QTL intervals and identifying the causative genes and developmental processes that underlie this trait. With advances in sequencing and genotyping technologies (e.g., RAD sequencing, reviewed by Rowe et al. 2011), this is not an insurmountable task.

My data reveal a complicated relationship between shape and integration. Specifically, I document a strong non-linear relationship between PC1 score (shape) and the magnitude of integration (Figure 2.3): Individuals who possess the most extreme jaw shape contribute more to the magnitude of integration while individuals with average shape contribute less. This is not surprising as PCA, by definition, describes coordinated shifts among phenotypic characters, and thus individuals with extreme positive or negative PC1 scores should exhibit the strongest correlation among traits. The observation that a shape QTL potentially mediates an epistatic interaction for phenotypic integration underscores the protracted, non-linear relationship between integration and shape. While the amount of variation explained by PC1 relative to other axes likely has the most pronounced influence on estimates of the overall magnitude of integration, phenotypic integration is the overall level of inter-correlation among traits (Olson & Miller 1958), and thus should also be influenced by covariation along other PCs. I did not detect significant QTL for variation along subsequent PC axes, which is likely an artifact of the limited power of this experimental design, but the relationship between integration and shape does

disappear after PC1 (not shown). In essence, by employing a statistical design that involves PCA, integration and shape are inherently coupled, but I maintain that they are measures of different aspects of phenotype variation. Most relevant to this study, they are distinct in that they map to different genomic regions in most of my QTL scans, which suggest they are regulated by different genetic factors. On one hand I detect QTL for shape variation, whereas on the other hand I also find largely distinct QTL for shape covariation. Both are critical for assessing the evolutionary potential of a complex trait.

This work complements and extends the recent investigations into the genetic basis of integration patterns in the cichlid mandible (Parsons et al. 2012). Whereas this previous work identified the pattern of integration for the cichlid mandible, and defined "modules" (i.e., internally integrated anatomical regions) within the jaw, here I explore the magnitude of integration within each module. Together these methods offer a hierarchical approach for investigating integration at the genetic level, wherein the genetic basis of the pattern of integration (i.e., modularity) is analyzed first, followed by an analysis of integration magnitudes within each predefined modules. These methods should address the reality of integration more directly than either does alone, and offer more proximate insights into the genetic basis of integration.

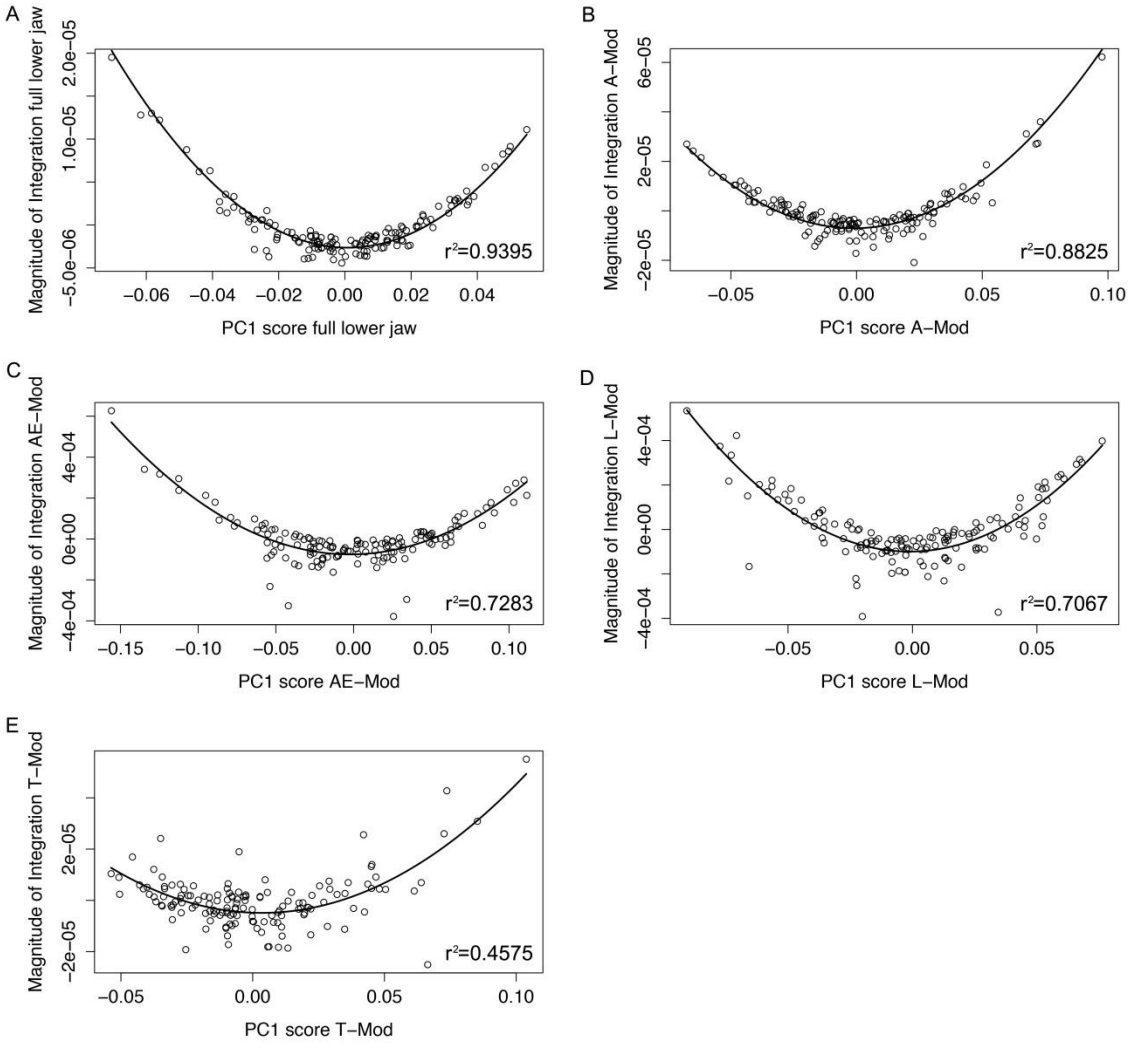

Figure 2.3. Relationships between shape and integration. Shown by ordinary least squares regression between PC1 score (shape) and individual magnitudes of integration. **A)** in the entire lower jaw; **B)** in the articular module; **C)** in the articular extension module; d in the lateral line module; e in the tooth-bearing module. From Yinan Hu et al. Evol Bio 2014;41:145-153.

This individual-level metric of integration is readily accessible for analyzing integration in other traits (Albertson et al. 2014), and the application extends beyond genetic analyses. With this new tool we are now able to quantify inter-individual variation in phenotypic integration, which can also be leveraged to understand how integration is inherited (i.e., through estimates of heritability), how integration evolves (i.e., through phylogenetic analysis, see Smith et al. 2015), and even how integration is tied to fitness. In other words, this tool can be used to gain an explicit understanding of how genetic and developmental architecture influences fitness by mediating shifts in phenotypic integration. This framework is what will ultimately lead to a comprehensive understanding of how integration influences organismal development, adaptation and evolution.

CHAPTER III

CRANIOFACIAL INTEGRATION AND EVOLUTION IN AN EXTREME ENVIRONMENT: THE ADAPTIVE DIVERSIFICATION OF ANTARCTIC NOTOTHENIOIDS

3.1 Introduction

Adaptive radiation refers to the rapid diversification of multiple lineages from a common ancestor as a consequence of adaptations to different ecological niches. It is an important evolutionary process that is thought to have produced much of the diversity of life on earth (Simpson 1953, Schluter 2000). Research programs in many well-known adaptive radiations such as Darwin's finches, East African cichlid fishes, Caribbean *Anolis* lizards, Hawaiian silverswords and so on have made significant contributions towards a better understanding of the processes and mechanisms through which diversity arises and is maintained over time (Baldwin & Sanderson 1998; Seehausen 2006; Grant & Grant 2008; Losos 2009).

Antarctic notothenioid fishes offer a rare example of an extensive adaptive morphological radiation in an extreme environment (Eastman & McCune 2000; Eastman 2005). During a series of cooling events over the past 40 million years, the dramatic drop in water temperature of the Southern Ocean has led to the local extinction of most near-shore fish lineages (Eastman 1993). However, the evolution of anti-freeze glycoproteins in notothenioids enabled these ancestrally benthic fishes to survive and adapt to the sub-zero temperatures (Matschiner et al. 2011). The evolution of "secondary pelagicism", the reinvasion of the pelagic foraging niche, has fostered their morphological evolution, as

they diversified to fill the newly available pelagic habitats (Eastman & DeVries 1981; Eastman 2005). Antarctic notothenioids now represent the primary teleost lineage in the Southern Ocean and are of fundamental importance to the local ecology (La Mesa et al. 2004). Insights from this clade would complement our current understanding of adaptive radiations from other system, which largely occur in tropical and sub-tropical regions.

Adaptive radiations are generally thought to occur via expanded ecological opportunities, which can be facilitated by the evolution of key-innovations, extinction of competitors, colonization of new habitats or other scenarios wherein empty niches become available to a lineage (Schluter 2000; Yoder et al. 2010). Diversification is then driven by a combination of divergent selection and relaxed stabilizing selection in the new environment. Widely embraced by evolutionary biologists since the modern synthesis, this classic neo-Darwinian view of evolution was built upon the assumption that the phenotypic variation that natural selection acts upon is largely determined by genes, and thus trait evolvability is a direct consequence of additive genetic variation (Pigliucci 2007; Laland et al. 2014). More recently however, with the emerging field of evo-devo, increasing attention has been devoted to characterizing how phenotypic variation originates. It is now widely accepted that not all genetic variation is expressed, rather, phenotypic variation may be biased or limited by developmental processes, such that evolution proceeds within the boundaries of developmental constraints (Hendrikse et al. 2007). Understanding how these constraints may affect evolvability is considered as a central question in the on-going "extended evolutionary synthesis" (Pigliucci 2009).

The covariation of traits (i.e. phenotypic integration) is predicted to exert profound influences on evolvability and is currently under heavy investigation (Klingenberg 2008; Klingenberg 2009; Young et al. 2010; Parsons et al. 2011; Hu et al. 2014; Collar et al. 2014). A group of integrated traits is considered a "module". Within the same module, shifts in one trait is predicted to be accompanied by corresponding changes in all other traits so that the entire module responds to selection in a coordinated fashion and results in a biased phenotypic response. Whether or not such bias is advantageous depends on the specific selection regimes imposed on the phenotype in question. Theoretical work (e.g., Klingenberg 2008) predicts that if selection favors shifts in a subset of traits in a module but not the rest, adaptation may be impeded. In fact, much recent work has found integration a constraining force in adaptive evolution (Young et al. 2010; Kimmel et al. 2012; Sears et al. 2013). But if selection happens to align with the pattern of integration and favors changes of the module as a whole, adaptation could occur rapidly. If true, this theoretical framework might explain why some lineages exhibit more extensive and/or rapid evolutionary radiations than others. However, empirical support for integration promoting adaptive diversification is rare. Moreover, the extent and efficiency through which integration itself can evolve across a clade is not well understood. Additional progress on this front is necessary to further our understanding of trait evolvability.

In this study, I show that variation in head shape aligns well with niche partitioning among notothenioid fishes, highlighting a key role for divergent selection with respect to foraging niche in this group. I document further the evolution of morphological integration among notothenioids, and show that the evolution of exceptionally high levels

of integration coincides with an accelerated rate of morphological evolution in the icefish family *Channichthyidae*. Taken together, I propose that shifts in integration can be considered as a key innovation in this group, and may have facilitated their radiation into pelagic feeding habitats.

3.2 Materials and methods

3.2.1 Fish specimen and phylogenetic data.

I collected 63 individuals of 21 notothenioid species during the Antarctic expedition B-037 with RV Laurence M. Gould in 2014. Specimen were fixed in 10% formalin on site, and preserved in 70% ethanol. Species were identified mostly by experienced research personnel with reference to Fishes of the Southern Ocean (Gon, O. & P.C. Heemstra 1990), ambiguities were verified by gene sequence from published data (Near et al. 2012). Additionally, 14 specimens of 9 notothenioid species from Harvard Museum of Comparative Zoology, and 1 *Pogonophryne scotti* specimen collected by H.W. Detrich in 2012 were also included in this study, consisting a total of 78 individuals and 30 species (Table 3.1). I re-derived the phylogeny of notothenioids based on Near et al. (2012), following the same methods described therein. In brief, a Bayesian phylogenetic analysis was performed on sequence data that includes 5 nuclear genes (RPS71, myh6, sh3px3, tbr1, and zic1) and 2 mitochondrial genes (nd2 and 16S rRNA) from 83 notothenioid species. BEAST analyses were run 5 times with $3*10^7$ generations each through the CIPRES Science Gateway (Miller et al. 2010), sampling at every 1000 generations. Resulting trees were combined with LogCombiner v2.2.1

(http://beast.bio.ed.ac.uk/LogCombiner), and summarized in TreeAnnotator v2.2.1 (http://beast.bio.ed.ac.uk/TreeAnnotator).

3.2.2 Morphological data collection and analyses.

3D-landmarks were obtained using the R package StereoMorph (Olsen & Westneat 2014). In brief, two cameras were arranged in fixed positions with overlapping field of views, and were calibrated using a standard checkerboard pattern. Landmarks were first digitized on regular 2D images from each camera and then reconstructed into 3D according to the calibration coefficients. 19 landmarks were recorded from one side of the head, and were then mathematically reflected across the midline assuming left-right symmetry, making a total of 35 landmarks (Figure 3.1; Table 3.2). Head width at multiple landmark positions were measured to assure the accuracy of reflection. Using routines in the Geomorph package (Adams & Otárola-Castillo 2013), the raw 3D landmark coordinates were aligned with a Generalized Procrustes Analysis. In order to control for common allometric effect across species, shape data were then regressed against centroid size of the head to obtain the residual shape component for subsequent analyses. Feeding habitat and specific diet items were based on published literature (Table 3.4). Modes of evolution were evaluated via a multivariate model-fitting approach with the R package mvMORPH (Clavel et al. 2015). Models were ranked according to the Akaike Information Criterion (Burnham & Anderson 2002).

taxa name	number of specimen	Source
Bathydraco_marri	2	B037
Chaenocephalus_aceratus	5	B037
Cryodraco_antarcticus	1	B037
Champsocephalus_gunnari	4	B037
Chionodraco_rastrospinosus	4	B037
Chaenodraco_wilsoni	3	B037
Dolloidraco_longedorsalis	2	B037
Dissostichus_mawsoni	1	B037
Pseudochaenichthys_georgian	2	B037
Gobionotothen_gibberifrons	3	B037
Harpagifer_antarcticus	2	B037
Lepidonotothen kempi	7	B037
Lepidonotothen_larseni	4	B037
Lepidonotothen_nudifrons	4	B037
Notothenia_coriiceps	6	B037
Notothenia_rossii	2	B037
Pagetopsis_macropterus	1	B037
Trematomus_eulepidotus	3	B037
Trematomus_hansoni	3	B037
Trematomus_scotti	3	B037
Pogonophryne_scotti	1	H.W. Detrich 2012
Chionobathyscus_dewitti	1	Harvard MCZ
Chionodraco_myersi	1	Harvard MCZ
Dacodraco_hunteri	2	Harvard MCZ
Eleginops_maclovinus	2	Harvard MCZ
Patagonotothen_tessellata	2	Harvard MCZ
Patagonotothen_cornucola	1	Harvard MCZ
Trematomus_borchgrevinki	2	Harvard MCZ
Trematomus_newnesi	2	Harvard MCZ
Trematomus_bernacchii	2	Harvard MCZ and B037

Table 3.1. List of notothenioid specimen used in this study. B037: fish specimen collected during Antarctic expedition B-037 in 2014. Harvard MCZ: specimen from Harvard Museum of Comparative Zoology. H.W. Detrich 2012: specimen collected by H.W.Detrich in 2012.

Landmark	description	position	Integration hypothesis 1	Integration hypothesis 2
1	most anterior-dorsal tip of opercle	Right	Posterior	Dorsal
2	most posterior point of the eye	Right	Posterior	Dorsal
3	most anterior point of the eye	Right	Anterior	Dorsal
4	most anterior-medial point of the maxilla	Right	Anterior	Dorsal
5	most anterior-lateral corner of the maxilla	Right	Anterior	Dorsal
6	most posterior-ventral tip of the maxilla	Right	Anterior	Ventral
7	most anterior-dorsal point of the A1 adductor mandibulae	Right	Anterior	Dorsal
8	quadrate-mandible joint	Right	Anterior	Ventral
9	insertion of the interopercular ligament on the retroarticular	Right	Anterior	Ventral
10	most anterior point of the A1-A2 division of adductor mandibulae	Right	Anterior	Ventral
11	most posterior point of the A1-A2 division of adductor mandibulae	Right	Posterior	Ventral
12	most posterior point of the A1-A3 division of adductor	Right	Posterior	Dorsal
13	most posterior-dorsal tip of opercle	Right	Posterior	Dorsal
14	most ventral point of the subopercle-interopercle joint	Right	Posterior	Ventral
15	most anterior point of the opercle-subopercle joint	Right	Posterior	Ventral
16	most anterior-dorsal origin of levator operculi muscle	Right	Posterior	Dorsal
17	most posterior-dorsal tip of the ascending process of the premaxilla	Midline	Anterior	Dorsal
18	most anterior tip of the premaxilla	Midline	Anterior	Dorsal
19	most anterior tip of the dentary	Midline	Anterior	Ventral
20	most anterior-dorsal tip of opercle	Left	Posterior	Dorsal
21	most posterior point of the eye	Left	Posterior	Dorsal
22	most anterior point of the eye	Left	Anterior	Dorsal
23	most anterior-medial point of the maxilla	Left	Anterior	Dorsal
24	most anterior-lateral corner of the maxilla	Left	Anterior	Dorsal
25	maxilla-articular joint	Left	Anterior	Ventral
26	most anterior-dorsal point of the A1 adductor mandibulae	Left	Anterior	Dorsal
27	quadrate-mandible joint	Left	Anterior	Ventral
28	insertion of the interopercular ligament on the retroarticular	Left	Anterior	Ventral
29	most anterior point of the A1-A2 division of adductor mandibulae	Left	Anterior	Ventral
30	most posterior point of the A1-A2 division of adductor mandibulae	Left	Posterior	Ventral
31	most posterior point of the A1-A3 division of adductor mandibulae	Left	Posterior	Dorsal
32	most posterior-dorsal tip of opercle	Left	Posterior	Dorsal
33	most ventral point of the subopercle-interopercle joint	Left	Posterior	Ventral
34	most anterior point of the opercle-subopercle joint	Left	Posterior	Ventral
35	most anterior-dorsal origin of levator operculi muscle	Left	Posterior	Dorsal

Table 3.2. List of landmarks included in the morphometrics analysis. Right side and midline landmarks were digitized via Stereomorph, landmarks on the left side were derived mathematically assuming left-right symmetry.

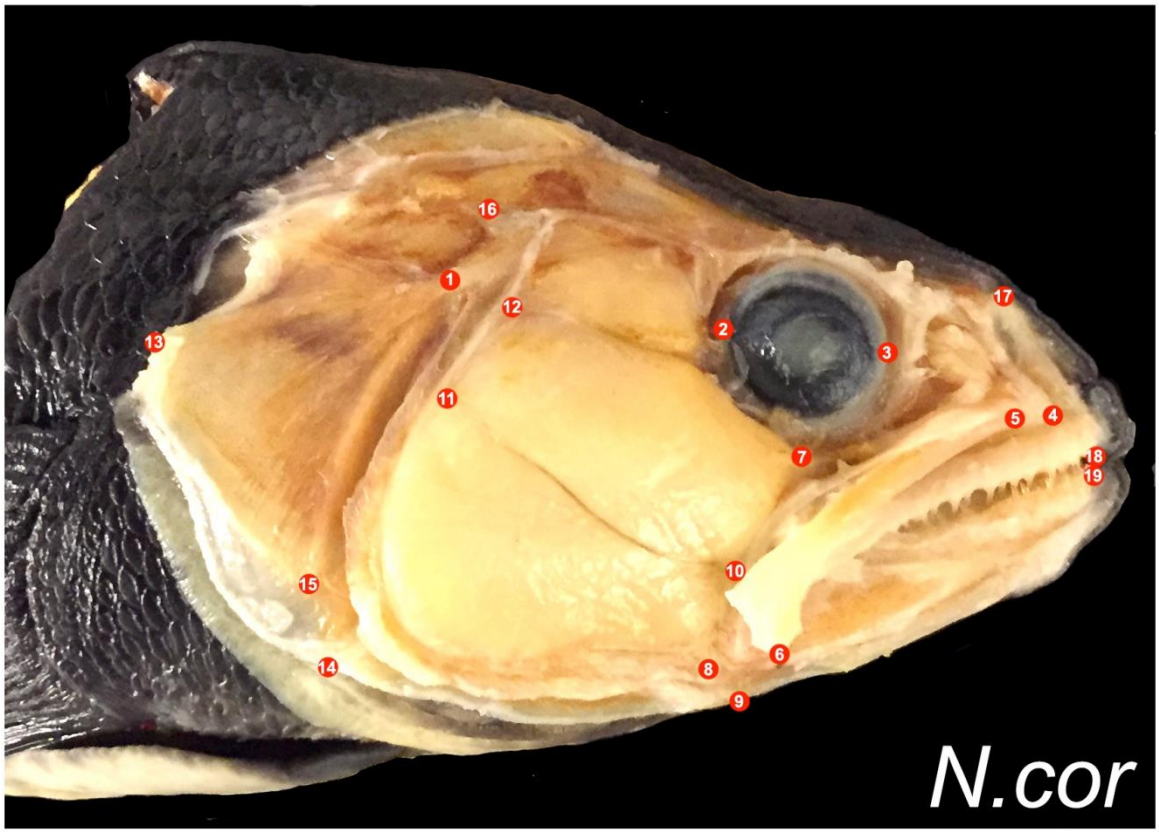

Figure 3.1. A visualization of the landmarks capture via Stereomorph. Picture shows the head of *Notothenia coriiceps*, Landmarks on the right side and midline (1-19, shown here) are directly digitized from specimen images via Stereomorph. Landmarks on the left side of the skull were mathematically derived assuming left-right symmetry. Specific position of landmarks can be found in Table 3.2.

3.2.3 Morphological integration analyses.

Hypotheses of morphological integration were evaluated with a recently developed method by Adams et al (Adams & Felice 2014). In brief, landmarks were divided into hypothetical modules (Table 3.2, and main text). The degree of covariation between the modules was then evaluated with a partial least squares approach while taking into account of phylogenetic relationships. Statistical significance was assessed via phylogenetic permutation with 3000 repeats. The magnitude of integration, measured as the variance of scaled eigenvalues of partial warp scores (i.e. percent variation explained by each PC axis), was assessed for each species via a recently developed jackknife approach (Hu et al. 2014). Integration was first measured for the whole dataset (78 individual from 30 species), and then re-measured after removing one individual. The difference between the two values provides an indirect measure of integration for that individual, as it represents the relative contribution from that particular individual to the overall magnitude of integration in that group. Average magnitude of integration for each species was then calculated from the individual measures.

3.2.4 Morphological disparity and evolutionary rate.

Morphological disparity through time was analyzed with the R package geiger (Harmon et al. 2008). A morphological disparity index (MDI) statistic was derived from the difference between observed disparity profile and a null model from Brownian motion simulations with 10,000 repeats. The most recent 20% of the tree was discarded to avoid tip over-dispersion, which may overestimate disparity due to incomplete coverage of terminal taxa (Harmon et al. 2003). Rate of morphological evolution was assessed using

routines in the R package geomorph (Adams & Otárola-Castillo 2013). All notothenioids were divided into an icefish group and non-icefish group. Evolutionary rate was calculated according to distances in morphospace between species in each group after phylogenetic transformation, statistical significance was assessed via randomized phylogenetic simulation with 1000 repeats.

3.3 Results and discussion

3.3.1 Divergence in skull shape is correlated with feeding habitat.

Variation in trophic morphology figures prominently in adaptive radiations as it's directly linked to resource use (Albertson et al. 2003b; Salzburger 2009; Yoder et al. 2010). In order to investigate patterns of morphological variation in the notothenioid head, I collected 3D shape data from 30 notothenioid species, which covers all major lineages within the clade. I found that the primary axis of shape variation in notothenioids corresponds to their feeding habitat (Figure 3.2). Species with extreme negative values on PC1 possess wide, robust skulls, short jaws, and feed predominantly along the bottom of the ocean. Alternatively, species with extreme positive values on PC1 have narrow, streamlined skulls, dramatically elongated jaws, and feed mainly on evasive prey items in the water column. Note that this end of the morphospace is largely defined by the white-blooded icefish clade (i.e., *Channichthyidae*).

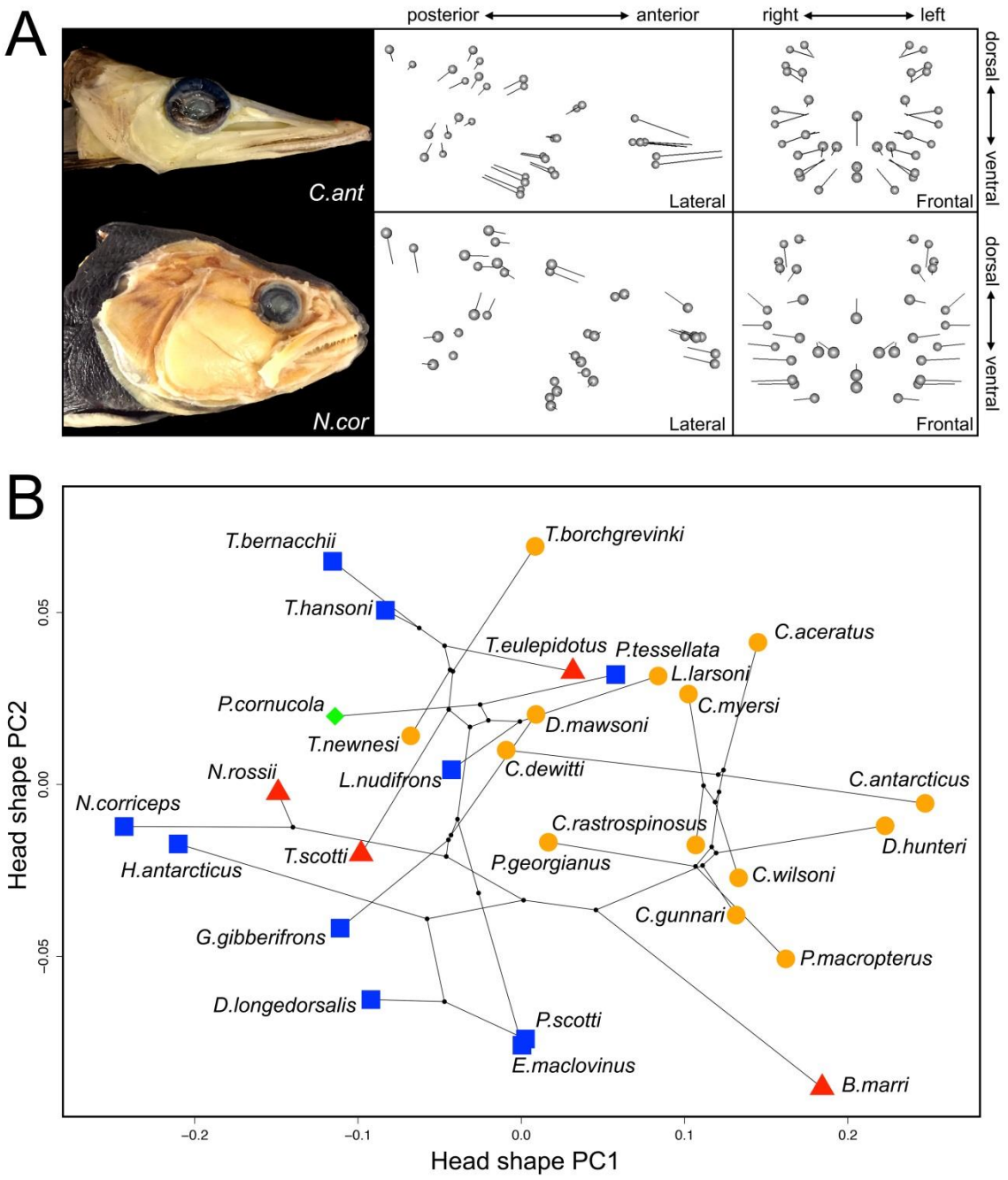

Figure 3.2. Morphological variation of the head corresponds to niche partitioning among notothenioids. A) Comparison of head shape between *Cryodraco antarcticus* and *Notothenia coriiceps*, which represent opposite ends of PC1. Ball and stick plot showing the vector displacements of corresponding landmarks from the mean head shape of all notothenioids analyzed in lateral and frontal views. B) Phylo-morphospace of notothenioids. PC1 explains 64.93% of the variance, PC2 explains 6.41%. Species are grouped according to feeding habitats. Blue square: benthic; Red triangle: intermediate; Orange circle: pelagic; Green diamond: unknown.

Model	log likelihood	AICc	Delta AICc	AICc Weight
OU-Diet3	26.11	-39.50	0.00	0.693
OU-Diet5	28.42	-37.25	2.25	0.225
OU-Single Peak	21.05	-35.10	4.40	0.077
Brownian Motion	16.98	-29.48	10.02	0.005
Early Burst	16.98	-26.96	12.54	0.001

Table 3.3. Comparison of alternative models of head shape evolution in notothenioids. Models are ordered from best to worst based on AICc scores. OU-Diet3: Ornstein-Uhlenbeck (OU) multi-peak model with species assigned to 3 categories according to feeding habitats (pelagic, intermediate and benthic); OU-Diet5: OU multi-peak model with species assigned to 5 categories according to feeding habitat and prey items (pelagic-large, pelagic-small, intermediate, benthic-soft, benthic-hard).

3.3.2 Divergent selection in different feeding habitats drives morphological evolution of the notothenioid head.

The close association between head shape and diet implies that morphological divergence is being driven, at least in part, by diversifying selection for different feeding habitats. To test this hypothesis, I used a multivariate model-fitting approach to examine the mode of evolution among these fishes (Table 3.3). I compared five hypothetical modes of evolution: 1) Brownian Motion model, a random-walk pattern of morphological evolution; 2) Early Burst model, in which most morphological variation was established early in the radiation; 3) Ornstein-Uhlenbeck (OU) single peak model, in which morphological variation was driven by selection towards one evolutionary optimum; 4) OU multi-peak 3 diet model, where morphological variation was driven by selection towards three feeding habitats (benthic, intermediate and pelagic); 5) OU multi-peak 5 diet model, in which I refined the 3 diet model and further partitioned both the benthic and pelagic peak into two separate peaks based on specific food items (Table 3.4).

taxa name	OU-Diet3	OU-Diet5
Bathydraco_marri	intermediate	intermediate
Chaenocephalus_aceratus	pelagic	pelagic-large
Cryodraco_antarcticus	pelagic	pelagic-large
Chionobathyscus_dewitti	pelagic	pelagic-large
Champsocephalus_gunnari	pelagic	pelagic-small
Chionodraco_myersi	pelagic	pelagic-large
Chionodraco_rastrospinosus	pelagic	pelagic-large
Chaenodraco_wilsoni	pelagic	pelagic-large
Dacodraco_hunteri	pelagic	pelagic-large
Dolloidraco_longedorsalis	benthic	benthic-soft
Dissostichus_mawsoni	pelagic	pelagic-large
Eleginops_maclovinus	benthic	benthic-soft
Pseudochaenichthys_georgian	pelagic	pelagic-large
Gobionotothen_gibberifrons	benthic	benthic-hard
Harpagifer_antarcticus	benthic	benthic-soft
Lepidonotothen kempi	benthic	benthic-soft
Lepidonotothen_larseni	pelagic	pelagic-small
Lepidonotothen_nudifrons	benthic	benthic-soft
Notothenia_coriiceps	benthic	benthic-hard
Notothenia_rossii	intermediate	intermediate
Patagonotothen_tessellata	benthic	benthic-soft
Patagonotothen_cornucola	UNKNOWN	UNKNOWN
Pagetopsis_macropterus	pelagic	pelagic-large
Pogonophryne_scotti	benthic	benthic-soft
Trematomus_bernacchii	benthic	benthic-hard
Trematomus_borchgrevinki	pelagic	pelagic-small
Trematomus_eulepidotus	intermediate	intermediate
Trematomus_hansoni	benthic	benthic-soft
Trematomus_newnesi	pelagic	pelagic-small
Trematomus_scotti	intermediate	intermediate

Table 3.4. Feeding habitat and dietary categories for each notothenioid species. pelagic-large: diet includes a considerable proportion of fish. pelagic-small: diet mainly includes small invertebrates. benthic-hard: benthic feeders capable of consuming hard-shelled invertebrates such as clams. benthic-soft: benthic feeders that feeds on relatively soft preys. References: (Gon & Vega 1990; Eastman 1993; La Mesa et al. 2004; Licandeo et al. 2006; La Mesa et al. 2007; Casaux & Barrera-oro 2013; Hüne & Vega 2015).

The best supported model was OU multi-peak 3 diet (Table 3.3), suggesting divergent selection for feeding habitat has shaped patterns of morphological evolution in this clade. The OU multi-peak 5 diet model was ranked the second highest, thus, both multi-peak models are significantly favored over all three single rate models, providing confidence in the conclusion that ecological opportunity in different feeding habitats was a major player during the notothenioid radiation. This association between morphological and behavioral divergence represents a characteristic feature of adaptive radiations in vertebrates. Well documented examples include beak size in Darwin's finches, limb length in *Anolis* lizards and jaw morphology in cichlid fishes (Grant 1999; Grant & Grant 2008; Cooper et al. 2010). Notably, the repeated adaptive radiations in African cichlids have resulted in a similar pattern of divergence compared to the notothenioids. In all three rift lakes, the primary axis of head shape variation in cichlids also aligns with a benthic-pelagic spectrum of feeding habitat in spite of two orders of magnitude difference in the age of each radiation (Cooper et al. 2010). This observation supports the prediction that this might represent a common selective axis among fish adaptive radiations (Cooper et al., 2010).

3.3.3 Notothenioids exhibit highly integrated skulls.

The first PC axis explains ~65% of the variance in head shape, while each of the remaining PCs explained less than 7% of the variance. This indicates that there is a significant amount of correlation among the landmarks examined, and suggests that the whole notothenioid skull may constitute an evolutionary module. To test this hypothesis, I used a partial least squares (PLS) based method to assess the level of covariation

between groups of landmarks while controlling for phylogenetic relationships (Adams & Felice 2014). The strength of covariation was assessed under two hypothesized patterns of modularity. The first is between the anterior and posterior regions of the skull (Table 3.2), and represents a functional hypothesis. Whereas the pre-orbital region of the skull is composed largely of the oral jaws and is involved primarily in prey capture, the posterior region is involved in feeding, respiration, and houses the brain and sensory organs. Previous work in mammal and fish (Drake & Klingenberg 2010; Parsons et al. 2011) supports modularity between these regions of the skull. The second model compares the dorsal and ventral regions of the skull (Table 3.2), and represents more of a developmental hypothesis. Whereas the dorsal portion of the skull contains the dermato- and viscerocranium, and develops from both neural crest and non-neural crest mesoderm, the ventral position of the skull is composed entirely of the neural crest-derived viscerocranium. Modularity in this dimension has also been shown in fish (Kimmel et al. 2012). Notably, I found no support for modularity in either dimension of the notothenioid skull. Instead, significant levels of covariation were detected between the hypothetical modules (hypothesis 1, anterior-posterior, $r_{PLS}=0.96$, $p<0.001$; hypothesis 2, dorsal-ventral, $r_{PLS}=0.90$, $p<0.003$).

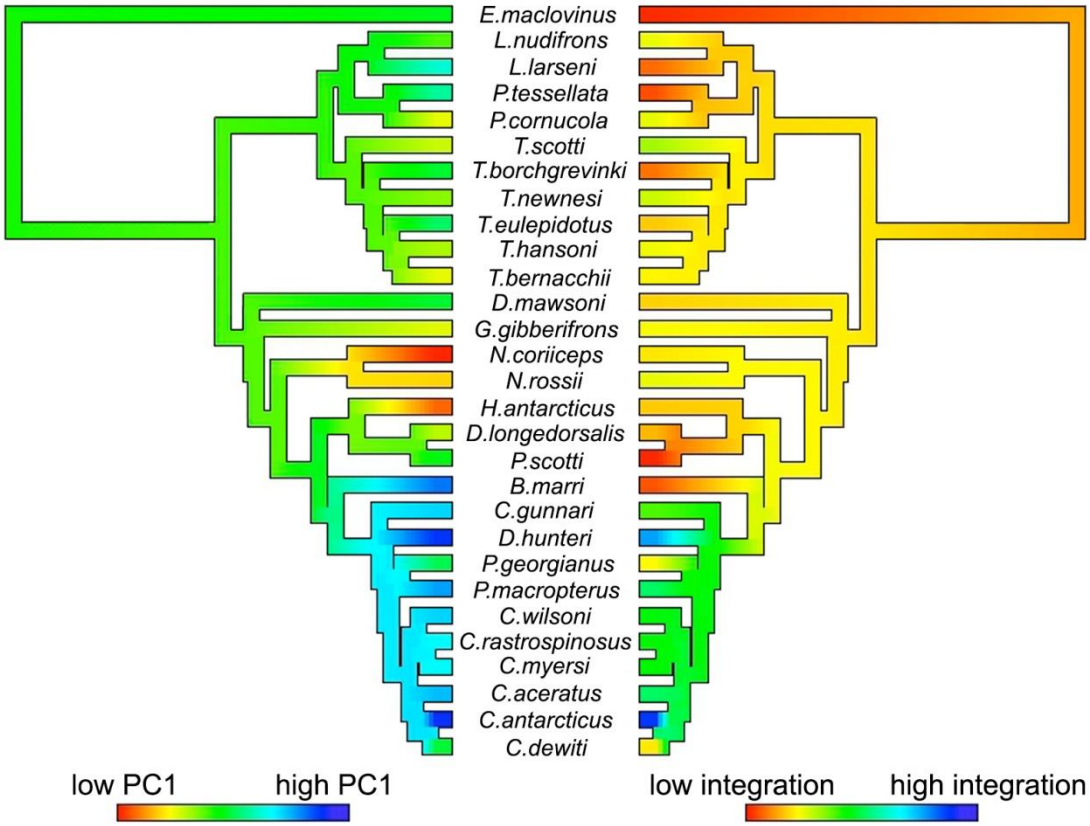

Figure 3.3. Ancestral state reconstruction of head shape PC1 and integration. Contour map phylogeny shows the estimated evolutionary history of each trait, produced with R package phytools (Revell 2012).

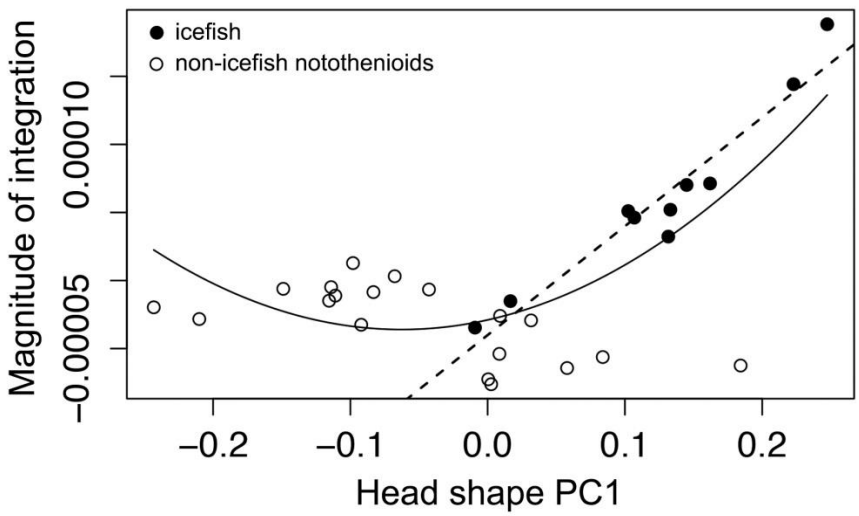

Figure 3.4. Relationship between head shape PC1 and magnitude of integration. Solid curve: quadratic regression across all notothenioids (r^2=0.5237, $p<1*10^{-4}$). Dashed line: linear regression within *Channichthyidae* (r^2=0.9143, $p<1*10^{-5}$).

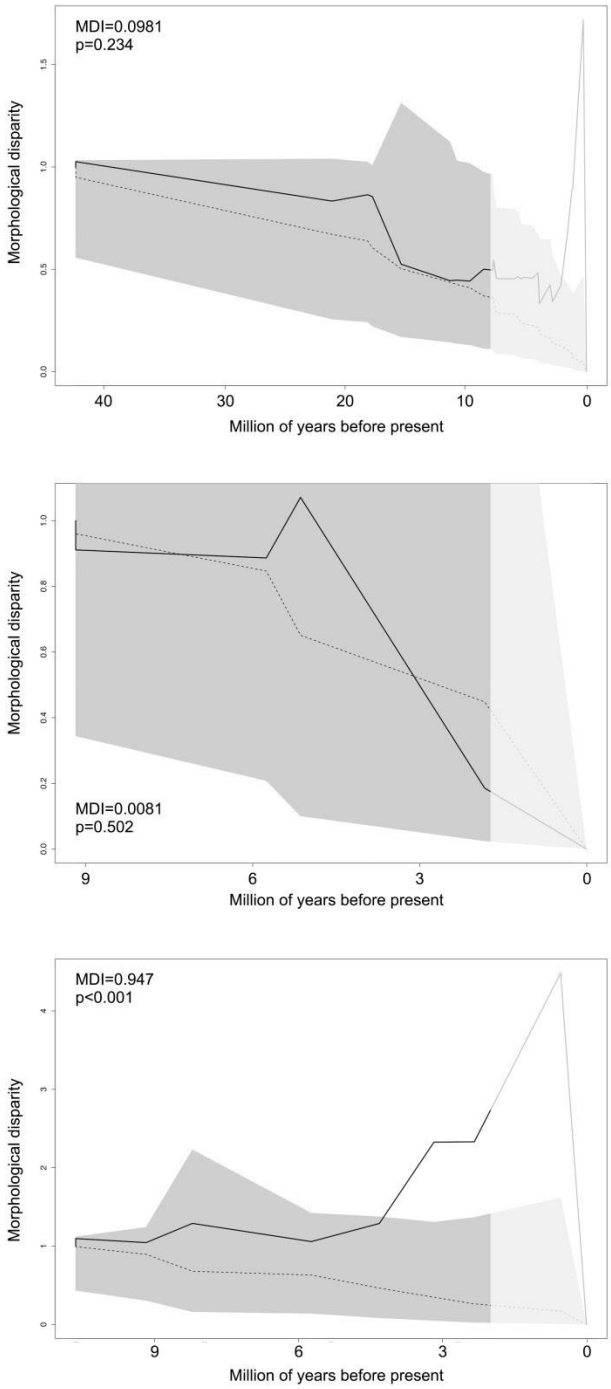

Figure 3.5. Morphological disparity through time. A) Disparity plot for all notothenioids. B) for *Trematomus*. C) for *Channichthyidae*. Estimated disparity through time is shown in solid line. Median disparity simulated under Brownian motion condition in dashed line and grey polygon represents 95% confidence interval of the simulated disparity.

To assess whether high levels of integration in the notothenioids skull is being driven by one or few lineages, I next used the jackknife-based approach developed in the previous chapter to assess the magnitude of integration for each individual (Hu et al. 2014), which allowed me to estimate the ancestral state and evaluate the evolution of integration as well as its relationship with shape variation across notothenioids. Several notable observations were made based on this analysis (Figure 3.3 and Figure 3.4). First, integration varied among closely related notothenioids species, which suggests that this trait can evolve over relatively brief time periods. Second, I found that the icefish lineage showed consistently high level of integration compared to the rest of notothenioids ($p<0.002$, t-test). Finally, I showed that morphological integration is correlated with shape. Across all notothenioids, the best supported relationship between shape (PC1) and integration is quadratic ($r^2=0.5237$, $p<1*10^{-4}$), such that species with extreme head shapes also exhibit the highest magnitude of integration. This nonlinear relationship between shape and integration has been noted in other lineages (Hu et al., 2014), and might reflect the inherent relationship between shape and integration when morphology is assessed via a PCA-based method. This is because by definition, PC1 captures the greatest amount of covariation among phenotypic characters, such that individuals with extreme PC1 scores are expected to contribute more to the overall degree of covariation and thus receive a higher integration score. Nevertheless, despite the statistical caveat, this approach is biologically valuable as it appears to measure different aspects of morphological variation which could lead to the discovery of distinct genetic underpinnings (Hu et al. 2014). Most relevant to this study, when only considering the icefish clade, I was able to uncover a strong linear correlation between shape and

integration (r^2=0.9143, $p<1*10^{-5}$). Interestingly, *Bathydraco marri*, a sister species to the Channighthyids, shows a very low level of integration, but has evolved a head shape similar to icefish (Figure 3.2; Figure 3.3), indicating that the tight correlation between integration and head shape is specific to *Channichthydae*. This is especially notable given that nearly half of the notothenioid craniofacial morphospace is defined by this lineage, and suggests that invasion of a pelagic foraging niche may have been facilitated by this shift in integration.

3.3.4 High magnitude of integration in icefish is associated with elevated shape diversity and accelerated rate of morphological evolution.

Next, I analyzed morphological disparity through time to evaluate the pattern of morphological diversification among notothenioids (Figure 3.5). Morphological disparity across the radiation as a whole is not significantly different from Brownian motion simulations, which suggests a steady increase in diversity over time. I further analyzed disparity in two subclades, *Trematomus* and *Channichthydae* (icefish), and found that while the disparity profile does not deviate from the null model in *Trematomus*, *Channichthydae* exhibited significantly higher levels of disparity, which indicates accelerated rates of morphological diversification with in this family. I then compared the rates of evolutionary change in head morphology between Channichthyds and the rest of notothenioids, and found that the skull shape is evolving at a significantly faster rate in this clade (sigmad.ratio=1.39, p=0.001). Taken together, these data shows that the high level of morphological integration coincides with rapid evolution of skull shape in the *Channichthyidae.*

3.3.5 Several key innovations underlie the origin and radiation of the notothenioid species flock.

The adaptive radiation of Antarctic notothenioids is accompanied by a series of key innovations (Eastman 2005; Matschiner et al. 2011; Matschiner et al. 2015). Arguably the most important one was the emergence of anti-freeze glycoproteins (AFGPs), which prevent the fish from freezing in the frigid Southern Ocean (at high latitudes, water temperature can remain less than -1.5°C all year long), and is thus critical to their survival in this extreme environment (Matschiner et al. 2011). A second innovation was the re-evolution of neutral or near-neutral buoyancy (Eastman & DeVries 1981). Ancestrally, all notothenioids lacked a swim bladder, which is suitable for a benthic lifestyle. However, during the evolution of secondary pelagicism, several lineages have evolved novel mechanisms to gain enough buoyancy and successfully invaded the pelagic foraging niches (Eastman 2005). For instance, to achieve an overall lower density, many pelagic notothenioids have evolved enlarged lipid sacs within the axial musculature, as well as reduced bone mineralization in the skeleton (Devries & Eastman 1978; Eastman & DeVries 1981; Eastman 2005). These novelties are able to compensate for the loss of the swim bladder and significantly reduce the amount of energy required for vertical migration into shallower water. In addition to these novel features, we argue that high magnitudes of integration could be interpreted as a key innovation unique to the icefish family *Channichthyidae*, as it accompanies their rapid evolution into a unique area of morphospace, and also their invasion into the largely unoccupied pelagic feeding habitat.

3.3.6 Integration as a key innovation among icefishes?

A high magnitude of phenotypic integration is generally considered to be a constraint on evolution, because any single mutation would cause corresponding changes in the entire module and would result in a higher probability of a deleterious outcome. However, theory predicts that if the direction of selection coincides with the axis of covariation (i.e. integration), accelerated evolution may result along that direction (i.e. evolutionary line of least resistance, Schluter 1996). I hypothesize that this is the case for the icefish lineage.

The *Channichthyidae* is a unique family of fish (Kock 2005) that is well-known for their loss of hemoglobin (Di Prisco et al. 2002), making them the only white-blooded vertebrate family on earth. Unlike all other notothenioid subclades, the entire Channichthyid family relies heavily on pelagic prey such as krill and fishes, and their mode of prey capture is also unique. Many icefish species exhibit a "benthopelagic" mode of foraging wherein they spend much of their time on or close to the ocean floor but venture into the pelagic zone to actively forage on schools of small fish and macroinvertebrates. Most benthopelagic notothenioids have non-protractible, elongate jaws, a wide gape, and many, small teeth. This design enables benthopelagic icefish to feed efficiently on krill and schools of small fishes by expanding their buccal cavity, overtaking, and sifting large mouthfuls of prey (Eastman 1993). This expanded ecological niche in icefish is also associated with accelerated lineage diversification (Near et al. 2004; Near et al. 2012). The *Channichthyidae* is now one of the most species-rich families with in the notothenioid clade, with at least 15 species (Kock 2005). The

exact age of this lineage remains elusive, mainly because of the lack of fossil records, but estimates range from 6 to 20 million years. By any measure, this is an extremely young family of fish, especially when one considers that development in the frigid Southern Ocean occurs at a very low pace. For instance, it can take up to 6 months for these fishes to hatch, and 5-8 years to reach sexual maturity (Kock 2005). Thus, even at the highest estimate of their age, the evolutionary history of icefish is on a similar scale of 2-4 million years that characterizes many radiations that have taken place in the tropics, where generation times are on the scale of 1-2 years.

It is tempting to speculate that elevated magnitudes of integration across notothenioids as a whole, and within icefish in particular may be due to shifts in early developmental patterning of the skull. The vertebrate pharyngeal skeleton is derived from neural crest cells, which migrate into a bilateral series of pharyngeal arches where they condense and differentiated into a conserved set of pharyngeal cartilages. These cartilages are the first elements of the vertebrate skull to develop, and patterning occurs along the dorsal-ventral and anterior-posterior axes through a conserved set of regulatory genes. It has been previously shown in notothenioids that the anterior and ventral cartilages of the pharyngeal skeleton develop earlier and grow faster than in other percomorph species (Albertson et al. 2010). In other words there is a bias toward the development of anterior and ventral elements of the pharyngeal skeleton. Even relatively short jawed, benthic notothenioids species exhibit this pattern, suggesting that this unique developmental program is ancestral to all notothenioids. However, the bias is greatly exaggerated in icefish where the development of highly elaborated ventral cartilages in larvae

foreshadow the elongated jaws in adults, providing clues to the developmental origins for this adaptive phenotype (Figure 3.6). I speculate that it is possible that such a dramatic change in the early patterning of the pharyngeal skeleton could serve to constrain variation across the remainder of the skull. For instance, it is possible that in order to remain functional, the development and growth of the icefish craniofacial complex is constrained to accommodate the early and exaggerated development of anterior and ventral elements. Thus, extreme jaw elongation via shifts in early developmental patterning events may account for the evolutionary success of the icefish, but as a consequence this mechanism may have led to coordinated variation throughout the rest of the head. To test this hypothesis one could compare early developmental patterning of an icefish species that exhibits high levels of integration and extreme shape along PC1 (e.g., *C. aceratus*) to that in a sister taxon to the icefish clade that still exhibits extreme PC1 values but low magnitudes of craniofacial integration (e.g., *B. marri*).

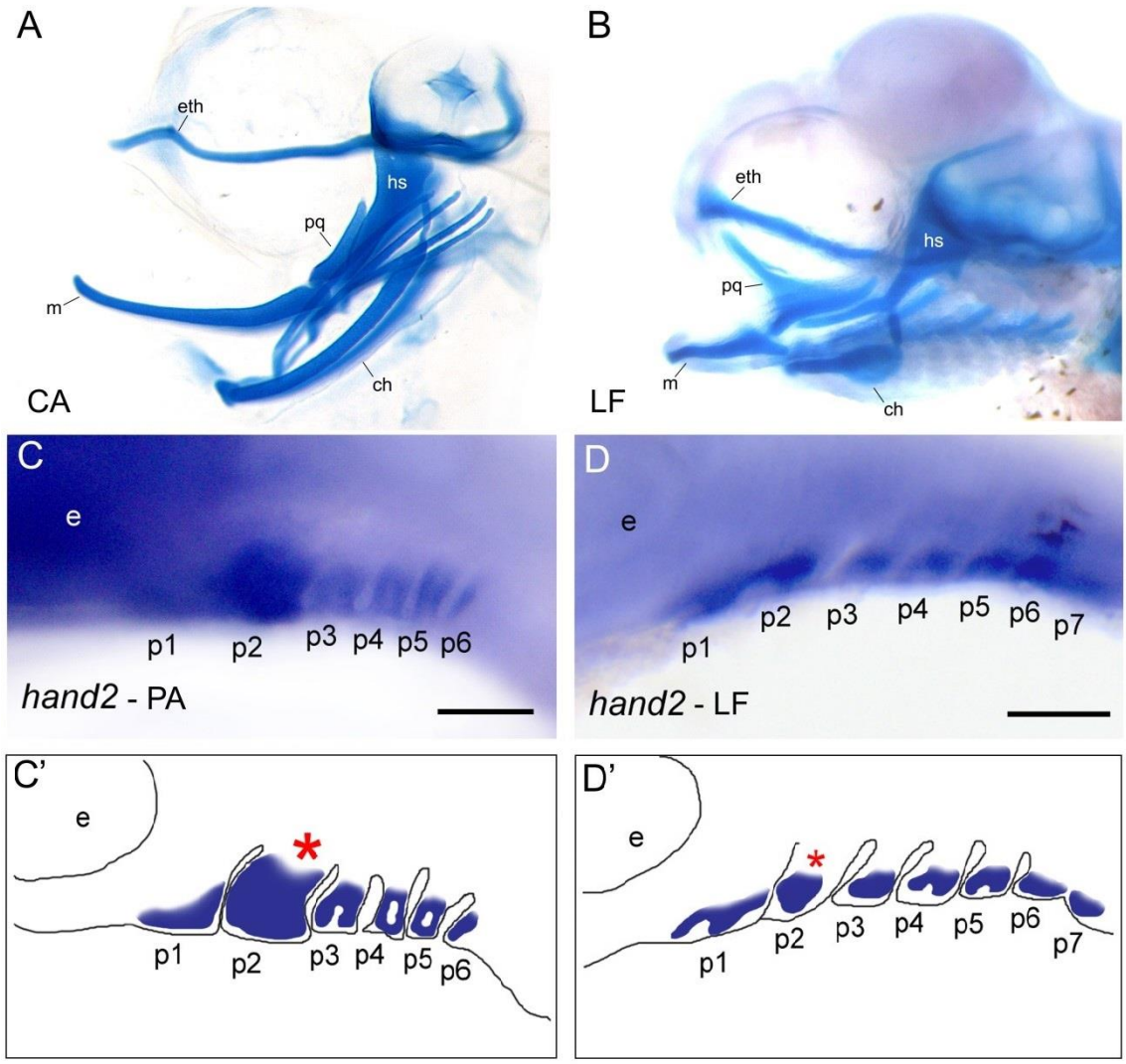

Figure 3.6. Biased development of anterior-ventral skeleton during early development in notothenioids. (A-B) Cleared and stained skeletal preperations. CA: icefish species *C.aceratus*. LF: cichlid species *L. fuelleborni*. Note the dramatically enlarged anterior-ventral cartilages in CA compared to LF. ch, ceratohyal; eth, ethmoid plate; hs, hyosymplectic; m, Meckel cartilage; pq, palatoquadrate. I hypothesize that this pattern is key to their highly integrated skull and that ventral patterning genes may be involved in this change. Differences in hand2 expression in the developing pharyngeal arches between notothenioids species P.antarcticum (C) and LF (D) support this hypothesis. p1-7, pharyngeal arches 1-7.

3.4 Conclusion

Understanding the determining factors of evolvability is an essential component in the on-going extended evolutionary synthesis (Pigliucci 2007; Pigliucci 2009). Although theory predicts that phenotypic integration could both limit and promote evolvability (Klingenberg 2008), empirical studies tend to find integration as a limiting factor to diversification (i.e. an "evolutionary constraint") (Young et al. 2010; Kimmel et al. 2012; Sears et al. 2013; Collar et al. 2014; Hu et al. 2014). In this study, I investigated patterns of morphological diversification in craniofacial skeleton among Antarctic notothenioids. I show that overall these fishes possess a highly integrated skull, and the magnitude of integration is especially high in the icefish family *Channichthyidae*. I further document an elevated rate of morphological evolution within this clade, which is accompanied by an unexpected tight correlation between integration and shape, indicating that integration might have promoted evolvability among the icefishes. The rapid evolution of head shape among the channichthyids leads to their occupation of a unique region in morphospace, which may have facilitated their invasion into the pelagic feeding habitat. Taken together, this study offers a rare example in which high magnitudes of integration are associated with rapid adaptation and a greater evolvability, shedding new light on the mechanisms that influence morphological diversification.

APPENDIX

R SCRIPT FOR MEASURING MAGNITUDE OF INTEGRATION ON INDIVIDUAL-LEVEL.

```
rm(list=ls())
#load data
setwd("working directory")
data<-read.csv("F2PWSizeRemovedForRAnalysis.csv",header=F)
data2<-as.matrix(data)
num.rows<-nrow(data2)
num.cols<-ncol(data2)
ComponentLoadings<-prcomp(data2)$rotation
PCscore<-data2%*%ComponentLoadings
#making the variance matrix, individual removed on the row, eigenvalue on column
VarMatrix<-matrix(0,nrow=num.rows,ncol=num.cols)
IndInt<-NULL   #vector for Individual integration value
IndVar<-NULL   #vector for Variance of eigenvalue as each individual was removed
TV<-NULL       #vector for eigenvalues
for (j in 1:num.cols)
{
TV[j]<-var(PCscore[,j])
}
TotVar<-var((TV)/sum(TV))   #standardized variance of eigenvalue of the whole
population
```

```
for (i in 1:num.rows)
{
jacknifeMatrix<-PCscore[-i,]
for (j in 1:num.cols)
{
VarMatrix[i,j]<-var(jacknifeMatrix[,j])
}
IndVar[i]<-var((VarMatrix[i,])/sum(VarMatrix[i,]))
IndInt[i]<-TotVar-IndVar[i]
}
write.csv(IndInt,file="Individual Integration level.csv")
```

BIBLIOGRAPHY

Abzhanov, A., Protas, M., Grant, B.R., Grant, P.R. & Tabin, C.J., 2004. Bmp4 and morphological variation of beaks in Darwin's finches. Science (New York, N.Y.), 305(5689), pp.1462–5.

Abzhanov, A., Kuo, W.P., Hartmann, C., Grant, B.R., Grant, P.R. & Tabin, C.J., 2006. The calmodulin pathway and evolution of elongated beak morphology in Darwin's finches. Nature, 442(7102), pp.563–7.

Abzhanov, A., Rodda, S.J., McMahon, A.P. & Tabin, C.J., 2007. Regulation of skeletogenic differentiation in cranial dermal bone. Development (Cambridge, England), 134(17), pp.3133–3144.

Adams, C.E. & Huntingford, F. a., 2002. The functional significance of inherited differences in feeding morphology in a sympatric polymorphic population of Arctic charr. Evolutionary Ecology, 16(1), pp.15–25.

Adams, D.C. & Otárola-Castillo, E., 2013. Geomorph: an R Package for the Collection and Analysis of Geometric Morphometric Shape Data E. Paradis, ed. Methods in Ecology and Evolution, 4(4), pp.393–399.

Adams, D.C. & Felice, R.N., 2014. Assessing trait covariation and morphological integration on phylogenies using evolutionary covariance matrices. PLoS ONE, 9(4).

Albertson, R.C. & Kocher, T.D., 2001. Assessing morphological differences in an adaptive trait: a landmark-based morphometric approach. The Journal of experimental zoology, 289(6), pp.385–403.

Albertson, R.C., Streelman, J.T. & Kocher, T.D., 2003a. Genetic Basis of Adaptive Shape Differences in the Cichlid Head. Journal of Heredity, 94(4), pp.291–301.

Albertson, R.C., Streelman, J.T. & Kocher, T.D., 2003b. Directional selection has shaped the oral jaws of Lake Malawi cichlid fishes. Proceedings of the National Academy of Sciences, 100(9), pp.5252–5257.

Albertson, R.C., Streelman, J.T., Kocher, T.D. & Yelick, P.C., 2005. Integration and evolution of the cichlid mandible: the molecular basis of alternate feeding strategies. Proceedings of the National Academy of Sciences of the United States of America, 102(45), pp.16287–92.

Albertson, R.C., Cresko, W., Detrich, H.W. & Postlethwait, J.H., 2008. Evolutionary mutant models for human disease. Trends in genetics : TIG, 25(2), pp.74–81.

Albertson, R.C., Yan, Y.-L., Titus, T. a, Pisano, E., Vacchi, M., Yelick, P.C., Detrich, H.W. & Postlethwait, J.H., 2010. Molecular pedomorphism underlies craniofacial skeletal evolution in Antarctic notothenioid fishes. BMC evolutionary biology, 10, p.4.

Albertson, R.C., Powder, K.E., Hu, Y., Coyle, K.P., Roberts, R.B. & Parsons, K.J., 2014. Genetic basis of continuous variation in the levels and modular inheritance of pigmentation in cichlid fishes. Molecular Ecology, 23(21), pp.5135–5150.

Arends, D., Prins, P., Broman, K. & Jansen, R., 2010. Tutorial-Multiple-QTL Mapping (MQM) Analysis. , pp.1–39.

Baldwin, B.G. & Sanderson, M.J., 1998. Age and rate of diversification of the Hawaiian silversword alliance (Compositae). Proceedings of the National Academy of Sciences of the United States of America, 95(16), pp.9402–9406.

Broman, K.W. & Sen, S., 2009. A Guide to QTL Mapping with R/qtl, New York, NY: Springer New York.

Burnham, K.P. & Anderson, D.R., 2002. Model Selection and Multimodel Inference K. P. Burnham & D. R. Anderson, eds., New York, NY: Springer New York.

Brugmann, S.A., Powder, K.E., Young, N.M., Goodnough, L.H., Hahn, S.M., James, A.W., Helms, J.A. & Lovett, M., 2010. Comparative gene expression analysis of avian embryonic facial structures reveals new candidates for human craniofacial disorders. Human Molecular Genetics, 19(5), pp.920–930.

Casaux, R. & Barrera-oro, E., 2013. Dietary overlap in inshore notothenioid fish from the Danco Coast , western Antarctic Peninsula. , 1, pp.1–8.

Chen, J.K., Taipale, J., Cooper, M.K. & Beachy, P. a, 2002. Inhibition of Hedgehog signaling by direct binding of cyclopamine to Smoothened service Inhibition of Hedgehog signaling by direct binding of cyclopamine to Smoothened. Genes & Development, (410), pp.2743–2748.

Chuong, C.-M., Patel, N., Lin, J., Jung, H.-S. & Widelitz, R.B., 2000. Sonic hedgehog signaling pathway in vertebrate epithelial appendage morphogenesis: perspectives in development and evolution. Cellular and Molecular Life Sciences, 57(12), pp.1672–1681.

Clavel, J., Escarguel, G. & Merceron, G., 2015. mvMORPH: an R package for fitting multivariate evolutionary models to morphometric data. Methods in Ecology and Evolution.

Collar, D.C., Wainwright, P.C., Alfaro, M.E., Revell, L.J. & Mehta, R.S., 2014. Biting disrupts integration to spur skull evolution in eels. Nature Communications, 5, p.5505.

Cooper, W.J. & Westneat, M.W., 2009. Form and function of damselfish skulls: rapid and repeated evolution into a limited number of trophic niches. BMC evolutionary biology, 9, p.24.

Cooper, W.J., Parsons, K., McIntyre, A., Kern, B., McGee-Moore, A. & Albertson, R.C., 2010. Bentho-pelagic divergence of cichlid feeding architecture was prodigious and consistent during multiple adaptive radiations within African rift-lakes. PloS one, 5(3), p.e9551.

Dalziel, A.C., Rogers, S.M. & Schulte, P.M., 2009. Linking genotypes to phenotypes and fitness: how mechanistic biology can inform molecular ecology. Molecular ecology, 18(24), pp.4997–5017.

Danley, P.D. & Kocher, T.D., 2001. Speciation in rapidly diverging systems: lessons from Lake Malawi. Molecular ecology, 10(5), pp.1075–86.

Devries, A. & Eastman, J., 1978. Lipid sacs as a buoyancy adaptation in an Antarctic fish. Nature, 271, pp.352–353.

Drake, A.G. & Klingenberg, C.P., 2010. Large-scale diversification of skull shape in domestic dogs: disparity and modularity. The American naturalist, 175(3), pp.289–301.

Dumont, E.R., Dávalos, L.M., Goldberg, A., Santana, S.E., Rex, K. & Voigt, C.C., 2012. Morphological innovation, diversification and invasion of a new adaptive zone. Proceedings. Biological sciences / The Royal Society, 279(1734), pp.1797–805.

Durie, C.J. & Turingan, R.G., 2004. The effects of opercular linkage disruption on prey-capture kinematics in the teleost fish Sarotherodon melanotheron. Journal of experimental zoology. Part A, Comparative experimental biology, 301(8), pp.642–53.

Eastman, J.T. & DeVries, A.L., 1981. Buoyancy adaptations in a swim-bladderless Antarctic fish. Journal of Morphology, 167(1), pp.91–102.

Eastman, J.T., 1993. Antarctic fish biology: evolution in a unique environment. Academic Press, San Diego.

Eastman, J.T. & McCune, a. R., 2000. Fishes on the Antarctic continental shelf: evolution of a marine species flock? Journal of Fish Biology, 57, pp.84–102.

Eastman, J.T., 2005. The nature of the diversity of Antarctic fishes. Polar Biology, 28(2), pp.93–107.

Fraser, G.J., Bloomquist, R.F. & Streelman, J.T., 2008. A periodic pattern generator for dental diversity. BMC biology, 6, p.32.

Fujimura, K. & Okada, N., 2007. Development of the embryo, larva and early juvenile of Nile tilapia Oreochromis niloticus (Pisces: Cichlidae). Developmental staging system. Development, growth & differentiation, pp.301–324.

Gans, C. & Northcutt, R.G., 1983. Neural crest and the origin of vertebrates: a new head. Science (New York, N.Y.), 220(4594), pp.268–73.

Gon, O. & P.C. Heemstra (eds). 1990. *Fishes of the Southern Ocean*. J.L.B. Smith Institute of Ichthyology, Grahamstown, 462 pp. 12pls.

Gould, S.J., 1982. Darwinism and the expansion of evolutionary theory. Science (New York, N.Y.), 216(4544), pp.380–387.

Grant, P.R. Ecology and Evolution of Darwin's Finches (Princeton Univ. Press, 1999)

Grant, P.R. and Grant, B.R. (2008) How and Why Species Multiply: The Radiation of Darwin's Finches, Princeton University Press

Hallgrímsson, B., & Hall, B.K. (2005). Variation and variability: Central concepts in biology. In B. Hallgrímsson & B. K. Hall (Eds.), Variation: A central concept in biology B (pp. 1–7). New York: Academic Press.

Hallgrímsson, B., Jamniczky, H., Young, N.M., Rolian, C., Parsons, T.E., Boughner, J.C. & Marcucio, R.S., 2009. Deciphering the Palimpsest: Studying the Relationship Between Morphological Integration and Phenotypic Covariation. Evolutionary Biology, 36(4), pp.355–376.

Hammond, C.L. & Schulte-Merker, S., 2009. Two populations of endochondral osteoblasts with differential sensitivity to Hedgehog signalling. Development (Cambridge, England), 136(23), pp.3991–4000.

Harmon, L.J., Schulte, J. a, Larson, A. & Losos, J.B., 2003. Tempo and mode of evolutionary radiation in iguanian lizards. Science (New York, N.Y.), 301(5635), pp.961–964.

Harmon, L.J., Weir, J.T., Brock, C.D., Glor, R.E. & Challenger, W., 2008. GEIGER: Investigating evolutionary radiations. Bioinformatics, 24(1), pp.129–131.

Harris, M.P., Williamson, S., Fallon, J.F., Meinhardt, H. & Prum, R.O., 2005. Molecular evidence for an activator-inhibitor mechanism in development of embryonic feather

branching. Proceedings of the National Academy of Sciences of the United States of America, 102(33), pp.11734–11739.

Helms, J. a & Schneider, R. a, 2003. Cranial skeletal biology. Nature, 423(6937), pp.326–331.

Hendrikse, J.L., Parsons, T.E. & Hallgrímsson, B., 2007. Evolvability as the proper focus of evolutionary developmental biology. Evolution & development, 9(4), pp.393–401.

Hu, Y., Parsons, K. & Albertson, R., 2014. Evolvability of the Cichlid Jaw: New Tools Provide Insights into the Genetic Basis of Phenotypic Integration. Evolutionary Biology, pp.145–153.

Hu, Y. & Albertson, R.C., 2014. Hedgehog signaling mediates adaptive variation in a dynamic functional system in the cichlid feeding apparatus. Proceedings of the National Academy of Sciences of the United States of America, 111(23), pp.8530–4.

Hüne, M. & Vega, R., 2015. Spatial variation in the diet of Patagonotothen tessellata (Pisces, Nototheniidae) from the fjords and channels of southern Chilean Patagonia. Polar Biology.

Ingham, P.W. & Fietz, M.J., 1995. Quantitative effects of hedgehog and decapentaplegic activity on the patterning of the Drosophila wing. Current biology : CB, 5(4), pp.432–440.

Irschick, D.J., Albertson, R.C., Brennan, P., Podos, J., Johnson, N. a, Patek, S. & Dumont, E., 2013. Evo-devo beyond morphology: from genes to resource use. Trends in ecology & evolution, pp.1–7.

Kimmel, C.B., Hohenlohe, P. a, Ullmann, B., Currey, M. & Cresko, W. a, 2012. Developmental dissociation in morphological evolution of the stickleback opercle. Evolution & development, 14(4), pp.326–37.

Klingenberg, C.P., 2008. Morphological Integration and Developmental Modularity. Annual Review of Ecology, Evolution, and Systematics, 39(1), pp.115–132.

Klingenberg, C.P., 2009. Morphometric integration and modularity in configurations of landmarks: tools for evaluating a priori hypotheses. Evolution & development, 11(4), pp.405–21.

Kocher, T.D., 2004. Adaptive evolution and explosive speciation: the cichlid fish model. Nature reviews. Genetics, 5(4), pp.288–98.

Kock, K.-H.H., 2005. Antarctic icefishes (Channichthyidae): a unique family of fishes. A review, Part I. Polar Biology, 28(11), pp.862–895.

Konings, A. (2001). Malawi cichlids in their natural habitat. El Paso, TX: Cichlid.

Koyama, E., Yamaai, T., Iseki, S., Ohuchi, H., Nohno, T., Yoshioka, H., Hayashi, Y., Leatherman, J.L., Golden, E.B., Noji, S. & Pacifici, M., 1996. Polarizing activity,Sonic hedgehog, and tooth development in embryonic and postnatal mouse. Developmental Dynamics, 206(1), pp.59–72.

Krauss, S., Concordet, J.P. & Ingham, P.W., 1993. A functionally conserved homolog of the Drosophila segment polarity gene hh is expressed in tissues with polarizing activity in zebrafish embryos. Cell, 75(7), pp.1431–1444.

Laland, K., Uller, T., Feldman, M., Sterelny, K., Müller, G.B., Moczek, A., Jablonka, E., Odling-Smee, J., Wray, G.A., Hoekstra, H.E., Futuyma, D.J., Lenski, R.E., Mackay, T.F.C., Schluter, D. & Strassmann, J.E., 2014. Does evolutionary theory need a rethink? Nature, 514(7521), pp.161–164.

Lauder, G., 1980. Evolution of the feeding mechanism in primitive actionopterygian fishes: a functional anatomical analysis of Polypterus, Lepisosteus, and Amia. Journal of Morphology, 317, pp.283–317.

Lauder, G., 1982. Patterns of evolution in the feeding mechanism of actinopterygian fishes. American Zoologist, 22(2), pp.275–285.

Lauder, G. & Liem, K., 1983. The evolution and interrelationships of the actinopterygian fishes. , 150(March 1983).

Licandeo, R.R., Barrientos, C. a. & González, M.T., 2006. Age, growth rates, sex change and feeding habits of notothenioid fish Eleginops maclovinus from the central-southern Chilean coast. Environmental Biology of Fishes, 77(1), pp.51–61.

Loh, Y.-H.E., Katz, L.S., Mims, M.C., Kocher, T.D., Yi, S. V & Streelman, J.T., 2008. Comparative analysis reveals signatures of differentiation amid genomic polymorphism in Lake Malawi cichlids. Genome biology, 9(7), p.R113.

Losos, J.B. (2009) Lizards in an Evolutionary Tree: Ecology and Evolution of Caribbean Anoles, University of California Press

Marroig, G. & Cheverud, J., 2005. Size as a line of least evolutionary resistance: diet and adaptive morphological radiation in New World monkeys. Evolution, 59(5), pp.1128–1142.

Matschiner, M., Hanel, R. & Salzburger, W., 2011. On the origin and trigger of the notothenioid adaptive radiation. PloS one, 6(4), p.e18911.

Matschiner, M., Colombo, M., Damerau, M., Ceballos, S., Hanel, R. & Salzburger, W., 2015. Extremophile Fishes,

Mayr, E. (1954). Change of genetic environment and evolution. In J. Huxley, A. C. Hardy,& E. B. Ford (Eds.), Evolution as a process (pp. 157–180). London: Allen & Unwin.

McCarthy, J.M. & Soh, G.S., 2011. Geometric Design of Linkages second., New York, NY: Springer New York.

La Mesa, M., Eastman, J.T. & Vacchi, M., 2004. The role of notothenioid fish in the food web of the Ross Sea shelf waters: a review. Polar Biology, 27(6), pp.321–338.

La Mesa, M., Eastman, J.T. & Licandro, P., 2007. Feeding habits of Bathydraco marri (Pisces, Notothenioidei, Bathydraconidae) from the Ross Sea, Antarctica. Polar Biology, 30(5), pp.541–547.

Miller, M. a., Pfeiffer, W. & Schwartz, T., 2010. Creating the CIPRES Science Gateway for inference of large phylogenetic trees. 2010 Gateway Computing Environments Workshop, GCE 2010.

Near, T.J., Pesavento, J.J. & Cheng, C.-H.C., 2004. Phylogenetic investigations of Antarctic notothenioid fishes (Perciformes: Notothenioidei) using complete gene sequences of the mitochondrial encoded 16S rRNA. Molecular phylogenetics and evolution, 32(3), pp.881–91.

Near, T.J., Dornburg, A., Kuhn, K.L., Eastman, J.T., Pennington, J.N., Patarnello, T., Zane, L., Fernández, D. a & Jones, C.D., 2012. Ancient climate change, antifreeze, and the evolutionary diversification of Antarctic fishes. Proceedings of the National Academy of Sciences of the United States of America, 109(9), pp.3434–9.

Neiffer, D.L. & Stamper, M.A., 2009. Fish sedation, analgesia, anesthesia, and euthanasia: considerations, methods, and types of drugs. ILAR journal / National Research Council, Institute of Laboratory Animal Resources, 50(4), pp.343–60.

Nomura, S. & Takano-Yamamoto, T., 2000. Molecular events caused by mechanical stress in bone. Matrix biology : journal of the International Society for Matrix Biology, 19(2), pp.91–6.

Olsen, A.M. & Westneat, M.W., 2014. StereoMorph: an R package for the collection of 3D landmarks and curves using a stereo camera set-up. Methods in Ecology and Evolution, p.n/a–n/a.

Olson, E.C., & Miller, R.L. (1958). Morphological integration. Chicago: University of Chicago Press.

Parsons, K.K.J. & Robinson, B.W.B., 2006. Replicated evolution of integrated plastic responses during early adaptive divergence. Evolution, 60(4), pp.801–813.

Parsons, K.J., Cooper, W.J. & Albertson, R.C., 2011. Modularity of the oral jaws is linked to repeated changes in the craniofacial shape of african cichlids. International journal of evolutionary biology, 2011, p.641501.

Parsons, K.J., Márquez, E. & Albertson, R.C., 2012. Constraint and opportunity: the genetic basis and evolution of modularity in the cichlid mandible. The American naturalist, 179(1), pp.64–78.

Parsons, K.J. & Albertson, R.C., 2013. Unifying and generalizing the two strands of evo-devo. Trends in ecology & evolution, 28(10), pp.584–91.

Pavlicev, M., Cheverud, J.M. & Wagner, G.P., 2009. Measuring Morphological Integration Using Eigenvalue Variance. Evolutionary Biology, 36(1), pp.157–170.

Pigliucci, M., & Preston, K. (Eds.). (2004). Phenotypic integration: Studying the ecology and evolution of complex phenotypes. New York: Oxford University Press.

Pigliucci, M., 2007. Do we need an extended evolutionary synthesis? Evolution; international journal of organic evolution, 61(12), pp.2743–9.

Pigliucci, M., 2009. An extended synthesis for evolutionary biology. Annals of the New York Academy of Sciences, 1168, pp.218–28.

Di Prisco, G., Cocca, E., Parker, S.K. & Detrich, H.W., 2002. Tracking the evolutionary loss of hemoglobin expression by the white-blooded Antarctic icefishes. Gene, 295(2), pp.185–191.

Revell, L.J., 2012. phytools: An R package for phylogenetic comparative biology (and other things). Methods in Ecology and Evolution, 3(2), pp.217–223.

Ribbink, A.J., Marsh, B.A., Marsh, A.C., Ribbink, A.C., & Sharp, B.J. (1983). A preliminary survey of the cichlid fishes of rocky habitats in Lake Malawi. South African Journal of Zoology, 18(3), 149–309.

Riopel, C., Robinson, B.W. & Parsons, K.J., 2008. Analyzing nested variation in the body form of Lepomid sunfishes. Environmental Biology of Fishes, 82(4), pp.409–420.

Roberts, R.B., Hu, Y., Albertson, R.C. & Kocher, T.D., 2011. Craniofacial divergence and ongoing adaptation via the hedgehog pathway. PNAS, 108(32), pp.13194–13199.

Rombough, P., 2002. Gills are needed for ionoregulation before they are needed for O(2) uptake in developing zebrafish, Danio rerio. The Journal of experimental biology, 205(Pt 12), pp.1787–94.

Rosas-Guerrero, V., Quesada, M., Armbruster, W.S., Pérez-Barrales, R. & Smith, S.D., 2011. Influence of pollination specialization and breeding system on floral integration and phenotypic variation in Ipomoea. Evolution; international journal of organic evolution, 65(2), pp.350–64.

Rowe, H.C., Renaut, S. & Guggisberg, a., 2011. RAD in the realm of next-generation sequencing technologies. Molecular Ecology, 20(17), pp.3499–3502.

Salzburger, W., 2009. The interaction of sexually and naturally selected traits in the adaptive radiations of cichlid fishes. Molecular ecology, 18(2), pp.169–85.

Schluter, D., 1996. Adaptive radiation along genetic lines of least resistance. Evolution, 50(5), pp.1766–1774.

Schluter, D., 2000. The ecology of adaptive radiation. Oxford: Oxford University Press 288 p.

Schoenebeck, J.J., Hutchinson, S. a., Byers, A., Beale, H.C., Carrington, B., Faden, D.L., Rimbault, M., Decker, B., Kidd, J.M., Sood, R., Boyko, A.R., Fondon, J.W., Wayne, R.K., Bustamante, C.D., Ciruna, B. & Ostrander, E. a., 2012. Variation of BMP3 Contributes to Dog Breed Skull Diversity T. Leeb, ed. PLoS Genetics, 8(8), p.e1002849.

Sears, K.E., Bianchi, C., Powers, L. & Beck, a L., 2013. Integration of the mammalian shoulder girdle within populations and over evolutionary time. Journal of evolutionary biology, 26(7), pp.1536–48.

Seehausen, O., 2006. African cichlid fish: a model system in adaptive radiation research. Proceedings. Biological sciences / The Royal Society, 273(1597), pp.1987–1998.

Simpson, G.G. (1953) The major features of evolution. New York: Colombia University Press. 434 p.

Smith, A.J., Nelson-Maney, N., Parsons, K.J., James Cooper, W. & Craig Albertson, R., 2015. Body Shape Evolution in Sunfishes: Divergent Paths to Accelerated Rates of Speciation in the Centrarchidae. Evolutionary Biology.

Streelman, J.T., Albertson, R.C. & Kocher, T.D., 2007. Variation in body size and trophic morphology within and among genetically differentiated populations of the cichlid fish, Metriaclima zebra, from Lake Malawi. Freshwater Biology, 52(3), pp.525–538.

Tanaka, M., Cohn, M.J., Ashby, P., Davey, M., Martin, P. & Tickle, C., 2000. Distribution of polarizing activity and potential for limb formation in mouse and chick embryos and possible relationships to polydactyly. Development (Cambridge, England), 127(18), pp.4011–4021.

Thompson, W.R., Rubin, C.T. & Rubin, J., 2012. Mechanical regulation of signaling pathways in bone. Gene, 503(2), pp.179–93.

Turner, G.F., Seehausen, O., Knight, M.E., Allender, C.J. & Robinson, R.L., 2001. How many species of cichlid fishes are there in African lakes? Molecular ecology, 10(3), pp.793–806.

Wainwright, P., 2004. A functional morphospace for the skull of labrid fishes: patterns of diversity in a complex biomechanical system. Biological Journal of the Linnean Society, pp.1–25.

Walker, J.A., 1997. Ecological morphology of lacustrine threespine stickleback Gasterosteus aculeatus L.(Gasterosteidae) body shape. Biological Journal of the Linnean Society, 61, pp.3–50.

Walker, M.B. & Kimmel, C.B., 2007. A two-color acid-free cartilage and bone stain for zebrafish larvae. Biotechnic & histochemistry : official publication of the Biological Stain Commission, 82(1), pp.23–8.

Westneat, M.W., 1994. Transmission of force and velocity in the feeding mechanisms of labrid fishes (Teleostei, Perciformes). Zoomorphology, 114(2), pp.103–118.

Westneat, M.W., 1995. Feeding, function, and phylogeny: analysis of historical biomechanics in labrid fishes using comparative methods. Systematic Biology, 44(3), pp.361–383.

Wu, P., Jiang, T.-X., Suksaweang, S., Widelitz, R.B. & Chuong, C.-M., 2004. Molecular shaping of the beak. Science (New York, N.Y.), 305(5689), pp.1465–6.

Wu, P., Jiang, T.-X., Shen, J.-Y., Widelitz, R.B. & Chuong, C.-M., 2006. Morphoregulation of avian beaks: comparative mapping of growth zone activities and morphological evolution. Developmental dynamics : an official publication of the American Association of Anatomists, 235(5), pp.1400–12.

Yoder, J.B., Clancey, E., Des Roches, S., Eastman, J.M., Gentry, L., Godsoe, W., Hagey, T.J., Jochimsen, D., Oswald, B.P., Robertson, J., Sarver, B. a J., Schenk, J.J., Spear, S.F. & Harmon, L.J., 2010. Ecological opportunity and the origin of adaptive radiations. Journal of Evolutionary Biology, 23(8), pp.1581–1596.

Young, N.M., Wagner, G.P. & Hallgrímsson, B., 2010. Development and the evolvability of human limbs. Proceedings of the National Academy of Sciences of the United States of America, 107(8), pp.3400–3405.